Received 26 February 2021; accepted 23 March 2021. Date of publication 1 April 2021; date of current version 14 April 2021.

Digital Object Identifier 10.1109/OJCOMS.2021.3070340

Analysis of Hierarchical Rate Splitting for Intelligent Reflecting Surfaces-Aided Downlink Multiuser MISO Communications

ANKUR BANSAL [1] (Member, IEEE), KESHAV SINGH [2] (Member, IEEE), AND CHIH-PENG LI [2] (Fellow, IEEE)

[1]Department of Electrical Engineering, Indian Institute of Technology Jammu, Jammu & Kashmir 181 221, India

[2]Institute of Communications Engineering, College of Engineering, National Sun Yat-sen University, Kaohsiung 80424, Taiwan

CORRESPONDING AUTHOR: K. SINGH (e-mail: keshav.singh@mail.nsysu.edu.tw)

This work was supported by the Ministry of Science and Technology of Taiwan under Grant MOST 109-2218-E-110-006 and Grant MOST 109-2221-E-110-050-MY3.

ABSTRACT An intelligent reflecting surface (IRS) is an emerging technology in the next-generation (B5G and 6G) wireless communications with the aim of improving the spectral/energy efficiency of the wireless networks. In this paper, we focus on multiple IRS-aided multiuser multiple-input single-output (MISO) downlink network, where each IRS is deployed near to the cell boundary of the cellular network in order to help the downlink transmission to the cell-edge users. To achieve the significant performance benefits provided by the rate-splitting (RS) transmission in multiuser scenario, two-layer hierarchical rate splitting (2L-HRS) technique is deployed at the base station (BS) to serve all the users. Furthermore, we propose an *On-Off* scheme for controlling the IRSs with practical phase shifts. In order to analyze the performance of the users, we derive the closed-form expressions of outage probability for both cell-edge users and near users. By extensive Monte Carlo simulations, we demonstrate that the proposed design framework outperforms the corresponding one-layer RS (1L-RS), the multiuser linear precoding (MU-LP) and 2L-HRS without IRS. In addition, we reveal the advantages of introducing RS-based IRS in improving the cell-users' performance. The impact of channel estimation errors due to imperfect channel state information, and the various network's parameters, such as the number of reflecting elements and the number of cell-users, on the network performance is demonstrated.

INDEX TERMS Intelligent reflecting surface (IRS), rate splitting (RS), multiple-input single-output (MISO), downlink, multiuser.

I. INTRODUCTION

IN THE era of the fifth generation (5G)-and-beyond communications, numerous technologies, such as massive multiple-input multiple-output (mMIMO), millimeter wave (mmWave) and ultra-dense deployments [1], [2], have emerged to fulfill the demand for high data rates and to support at least 100 billion ubiquitous wireless device connectivity. However, huge signal processing complexity, complex and time-varying wireless communication environment, implementation hardware cost and high energy consumption are major bottlenecks for these technologies. Consequently, intelligent reflecting surface (IRS), which will play a pivotal role in the next-generation (i.e., B5G and 6G) wireless networks [3]–[6], has recently emerged as an important cost-and-energy efficient technology to improve the spectrum efficiency of the cellular networks with minimal power depletion [7]–[24].

An IRS is a reconfigurable intelligent and software-controlled metasurfaces consisting of passive elements, wherein each element independently reflects the incident electromagnetic wave after adjusting the phase of each passive element [7]–[24]. Recently, several works on IRS-aided communications have been reported [10], [12]–[29]. The authors in [10] have discussed the latest research

activities in the areas of IRS-assisted wireless networks and highlighted the open research problems, while in [12], the large intelligent surfaces (LIS)-space shift keying and LIS-spatial modulation schemes have been investigated to enhance the network spectral efficiency along with signal quality at the end user. While in [13], an energy-efficient resource allocation scheme have been investigated for downlink multi-user communication systems, the authors in [14] have studied the emerging research field of reconfigurable intelligent surface (RIS)-empowered smart radio environments (SREs) and highlighted the most suitable applications of RISs in wireless networks along with presenting an electromagnetic-based communication-theoretic framework for analyzing and optimizing metamaterial-based RISs. The work [16] has proposed an enexact-alternative-optimization method to design the optimal transmit beamforming vectors at the base stations and the reflecting beamforming vectors at the IRS. Further, the resource allocation scheme has been studied in [18] for IRS-aided full duplex cognitive radio networks. While a non-orthogonal multiple access (NOMA) transmission scheme has been proposed in [21], [22], the beamforming design algorithms have been studied in [23]–[29]. For example: an IRS-aided single-cell wireless system have been studied in [23] with discrete phase shifters where a single IRS is deployed to help in the communications between a multi-antenna access point (AP) and multiple single-antenna users, while by jointly optimizing the active transmit precoders at the AP and the passive reflect phase shifts at all IRSs, the transmit power at the AP has been minimized in [24]. The authors in [25] have proposed a robust beamforming algorithm for IRS-assisted multi-user multiple-input single-output (MISO) network, whereas [26] has considered an IRS-assisted multi-cell multiple-input multiple-output (MIMO) network and focused on maximizing the weighted sum rate by jointly optimizing the active transmit precoder matrix at the base stations (BSs) and the phase-shift matrix at the IRS. Furthermore, the passive beamforming and information transfer strategy has been developed in [29] for IRS-assisted multiuser MIMO networks. However, none of the authors in [23]–[29] have analyzed the performance of rate-splitting multiple access (RSMA) based IRS-assisted communication network and thus, it motivates us to focus on this problem.

In the last few years, rate splitting (RS) has emerged as a remedy for improving the spectrum efficiency [30]–[36]. For instant, the authors in [30] have highlighted recent advancements in RS specially for MIMO networks, while the advantages of RSMA over NOMA technology have been illustrated in [32]. One of the most important characteristic of RSMA is that it partially decodes interference and partially treats interference as noise through the split into common and privates messages, whereas the NOMA completely relies on SIC and fully decodes interference. In addition, The NOMA is more suited to overloaded networks whereas the RSMA is suitable for all type of network loads. The techniques for stream combining and linear precoder design have been investigated in [34] for RS in multiuser MIMO systems. Moreover, to optimize the precoders, message splits, time slot allocation along with relaying user scheduling, the authors in [36] have formulated a max-min fairness problem of a K-user cooperative RS in MISO network. Similar to [36], the authors in [37] have adopted a RS strategy and developed a precoder design algorithm for maximizing minimum of all clusters rates in multi-group multicasting. However, to the best of the authors knowledge, the performance analysis of RS-based IRSs-aided multiuser MISO networks has not yet been investigated in the literature.

Inspire by the aforementioned discussions, in this paper we consider a multiuser MISO downlink network, where multiple IRS are deployed near to the cell boundary of the cellular network in order to assist the downlink transmission to cell-edge users and deploy two-layer hierarchical rate splitting (2L-HRS) at the BS. In the light of existing work [10], [12] [29], the major contributions of this work are outlined as follows.

- We primarily emphasis on multiple IRS-aided downlink MISO hierarchical RS (HRS) network wherein numerous IRS are deployed near to the cell boundary of the cellular network for serving the cell-edge users. To achieve the significant performance benefits provided by RS transmission specially in multiuser scenario, we deploy 2L-HRS transmission strategy at the BS.
- We propose an *On-Off* scheme for controlling the IRSs with *practical phase shifts*. Next, to analyze the performance of the users, we derive the closed-form expressions of outage probability for both cell-edge users and near users by considering both common as well as private data signal-to-interference-plus-noise ratio (SINR).
- By extensive Monte Carlo simulations, we validate the effectiveness of the proposed scheme and demonstrate that the proposed design framework outperforms the corresponding one-layer RS (1L-RS), the multiuser linear precoding (MU-LP) and 2L-HRS without IRS. In addition, we show the advantages of introducing RS-based IRS in improving the cell-users' performance.
- Moreover, we demonstrate the impact of channel estimation errors because of imperfect channel state information and the various network's parameters, such as the number of reflecting elements and the number of cell-users, on the network performance.

Organization: The rest of the paper is structured as follows. The system model is described in Section II. Section III presents the SINRs expressions for the considered HRS framework. While the proposed on-off scheme for controlling the IRS with practical phase shifts is illustrated in Section IV, outage analysis for IRS-aided HRS is depicted in Section V. In Section VI, numerical results are presented. At last, conclusions are drawn in Section VII.

Notations: The following notations are used throughout the paper. The lowercase and uppercase boldface letters (e.g.,

TABLE 1. Table of main notations.

Notations	Description
K	Total number of users.
M	Total number of non-overlapping groups.
N_r	Total number of reflecting elements.
N_s	Total number of antennas at the BS.
$\mathbf{x}$	Combined data vector.
$\mathbf{P}$	Precoder matrix.
$\mathbf{p}_{\mathbb{K}_m}$	Precoding vector for common-to-group data stream $x_{\mathbb{K}_m}$ for group G_m.
$\mathbf{p}_k$	Precoding vector for private data stream x_k.
$\mathbf{g}_q$	Channel between the BS and the q-th NU.
$\mathbf{H}_m$	Channel matrix between the BS and IRS$_m$.
$\mathbf{f}_{m,k}$	Channel vector between IRS$_m$ and the k-th CEU in group G_m.
$\mathbf{\Phi}_m$	Diagonal matrix containing the reflected amplitude and reflected phase shift values at IRS$_m$.
$\beta_{\min}$	Minimum reflection amplitude.
φ_n	Continuous phase of the incoming signal at the n-th active reflecting element.
$\beta_n(\varphi_n)$	Phase dependent reflection amplitude of n-th active element.
$\mathcal{P}_B$	Transmit power budget for the BS.

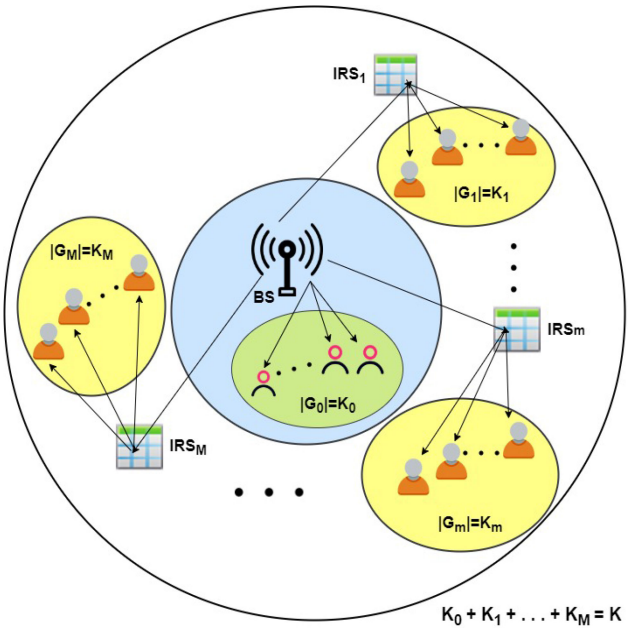

FIGURE 1. System Model for RS-based IRS assisted downlink MISO system with K users and M IRSs.

a and **A**) are used to denote a vector and a matrix, respectively. $(\cdot)^{\mathrm{H}}$ is defined for complex conjugate. The matrix $\mathbf{I}_M$ denotes an $M \times M$ identity matrix. $\mathbf{Tr}[\mathbf{A}]$ is the trace of a matrix $\mathbf{A}$ and $||\cdot||^2$ used to denote the square-norm. Besides, the list of main notations utilized in this paper are depicted in Table 1.

II. SYSTEM MODEL

We consider a downlink multi-user scenario as illustrated in Fig. 1 where a multi-antenna BS (with N_s antennas) utilizes rate splitting to serve multiple single antenna users. Let us consider a total of K single antenna users indexed by a set $\mathbb{K} = \{1, 2, \ldots, K\}$. We divide these K users into $M + 1$ groups,[1] denoted as G_m, $m \in \mathbb{M}$, where $\mathbb{M} = \{0, 1, \ldots, M\}$. The users having a direct link with BS, i.e., near users (NUs), are grouped into a single group G_0, whereas M non-overlapping groups are formed to divide all the cell-edge users (CEUs), i.e., the users with no direct connection from the BS. Each group consists a subset of users, $\mathbb{K}_m \subset \mathbb{K}$, such that $\mathbb{K}_m \cap \mathbb{K}_n = \emptyset$, $m \neq n$, $m, n \in \mathbb{M}$. If we assume that the cardinality of m-th subset is K_m, i.e., $|\mathbb{K}_m| = K_m$, them the groups satisfy $\sum_{m\in\mathbb{M}} |\mathbb{K}_m| = K$.

The BS communicates with a cell-edge group (CEG) $G_{m'}$ $m' \in \mathbb{M}'$, where $\mathbb{M}' = \{1, 2, \ldots, M\}$ through an IRS consisting of N_r reflecting elements. It is assumed that only the signals reflected by the IRS once are considered while those reflected by IRS for two and more times are ignored. The BS utilizes two-layer hierarchical rate splitting (2L-HRS) technique to serve all the users as explained below.

1. User grouping is a well known technique for the reduction of latency and interference [38], [39]. In this work, we assume that there exists a method [38], [39] to group the users based on the location in order to control the interference and we are provided with grouped users.

A. TWO-LAYER HIERARCHICAL RATE SPLITTING (2L-HRS)

In this technique, the BS splits the message of each user into three part-messages known as private, common and common-to-group part-messages. Similar to 1L-RS, the common part-messages of all the users are jointly encoded to obtain a common data stream of order K intended to all the users, and the private part-messages of each user is separately encoded to obtain K different 1-order private data streams intended to individual user. In addition to this, common-to-group part-messages of the users in a group G_m, $m \in \mathbb{M}$ are also jointly encoded to get a K_m-order data stream intended for the users in G_m only.

Let the combined data vector to be sent by the BS using 2L-HRS is $\mathbf{x} = [x_{\mathbb{K}}, x_{\mathbb{K}_0}, x_{\mathbb{K}_1}, \ldots, x_{\mathbb{K}_M}, x_1, x_2, \ldots, x_K]^T$, where $x_{\mathbb{K}}$ is the common data stream of order K, $x_{\mathbb{K}_m}$, $m \in \mathbb{M}$ represents the K_m-order common-to-group data stream to be decoded by the users in G_m, and x_k, $k \in \mathbb{K}$ is the unit-order private data stream corresponding to k-th user. We also assume unity average power constraint such that $\mathbf{Tr}[\mathbf{x}\mathbf{x}^{\mathrm{H}}] = 1$. The data vector $\mathbf{x}$ is linearly precoded with the help of an $N_s \times (K + M + 2)$ precoder matrix $\mathbf{P} = [\mathbf{p}_{\mathbb{K}}, \mathbf{p}_{\mathbb{K}_0}, \mathbf{p}_{\mathbb{K}_1}, \ldots, \mathbf{p}_{\mathbb{K}_M}, \mathbf{p}_1, \mathbf{p}_2, \ldots, \mathbf{p}_K]$, where the column vector $\mathbf{p}_{\mathbb{K}}$ precodes the common data stream $x_{\mathbb{K}}$, the column vector $\mathbf{p}_{\mathbb{K}_m}$ is used as a precoding vector for common-to-group data stream $x_{\mathbb{K}_m}$ for group G_m, and vector $\mathbf{p}_k$ is the precoding vector for private data stream x_k. The

data vector broadcasted by the BS can therefore be given as

$$\mathbf{s} = \mathbf{P}\mathbf{x} = \mathbf{p}_{\mathbb{K}} x_{\mathbb{K}} + \sum_{m\in\mathbb{M}} \mathbf{p}_{\mathbb{K}_m} x_{\mathbb{K}_m} + \sum_{k\in\mathbb{K}} \mathbf{p}_k x_k. \tag{1}$$

We assume a total transmit power constraint at the BS as $\mathbf{Tr}[\mathbf{P}\mathbf{P}^{\mathrm{H}}] \leq \mathcal{P}_B$.

B. DATA TRANSMISSION

The signal received at the q-th NU, $q \in \mathbb{K}_0$ can be given as

$$y_q = \mathbf{g}_q^{\mathrm{H}}\mathbf{s} + e_q, \tag{2}$$

where $\mathbf{g}_q$ denotes the $1 \times N_s$ channel vector between the BS and the q-th NU and e_q is the zero mean AWGN at the q-th NU in group G_0 with variance σ^2. Let all the elements of vector $\mathbf{g}_q$ are independent and identically distributed (i.i.d.) as zero mean complex Gaussian (ZMCG) random variables with variance Ω_g. Assuming that IRS$_m$ is placed close to m-th group G_m, $m \in \mathbb{M}'$ so that the only the CEUs in group G_m can hear from it. The received signal at the k-th CEU, $k \in \mathbb{K}$, $k \in \mathbb{K}_m$, $m \in \mathbb{M}'$ obtained through the m-th IRS can be written as

$$y_k = \mathbf{f}_{m,k}^{\mathrm{H}} \Phi_m \mathbf{H}_m \mathbf{s} + e_k, \tag{3}$$

where $\mathbf{H}_m$ denotes the $N_r \times N_s$ channel matrix between the BS and IRS$_m$, $\mathbf{f}_{m,k}$ denotes the channel vector between IRS$_m$ and the k-th CEU in group G_m. All the channel coefficients in matrix $\mathbf{H}_m$ and vector $\mathbf{f}_{m,k}$ are assumed to be i.i.d. as ZMCG random variables with variances Ω_h and Ω_f, respectively. The variable e_k denotes the zero mean AWGN at the receiving antenna of the CEU having variance σ^2. The transmit SNR can therefore be defined as $\rho_B = \frac{\mathcal{P}_B}{\sigma^2}$. Matrix Φ_m is a $N_r \times N_r$ diagonal matrix containing the reflection coefficients of each reflecting element at IRS$_m$ and can be defined as

$$\Phi_m = \mathrm{Diag}\Big(\beta_{m,1}(\varphi_{m,1})e^{j\varphi_{m,1}}, \beta_{m,2}(\varphi_{m,2})e^{j\varphi_{m,2}}, \ldots, \beta_{m,N_r}(\varphi_{m,N_r})e^{j\varphi_{m,N_r}}\Big), \tag{4}$$

where $\varphi_{m,n}$ and $\beta_{m,n}(\varphi_{m,n})$, $n = 1, 2, \ldots, N_r$, denote the phase shift and the phase dependent reflection amplitude at n-th reflecting element of IRS$_m$. If we write the elements of diagonal matrix Φ_m in a column vector, denoted by $\boldsymbol{\phi}_m$, and define a diagonal matrix $\mathbf{F}_{m,k}$ containing the elements of vector $\mathbf{f}_{m,k}$, then we can rewrite (3) as

$$y_k = \phi_m^{\mathrm{H}} \mathbf{F}_{m,k} \tilde{\mathbf{H}} \mathbf{x} + e_k, \tag{5}$$

where $\tilde{\mathbf{H}} = \mathbf{H}_m\mathbf{P} = [\mathbf{h}_{\mathbb{K}}, \mathbf{h}_{\mathbb{K}_0}, \ldots, \mathbf{h}_{\mathbb{K}_M}, \mathbf{h}_1, \ldots, \mathbf{h}_K]$ with each vector $\mathbf{h}_i = \mathbf{H}_m\mathbf{p}_i$. A maximum ratio transmission (MRT) can be utilized to initialize private precoders of RS, while singular value decomposition (SVD) can be utilized to initialize the common precoder [32], [33]. However, for tractability of the analysis and in order to satisfy the transmit power constraint, we consider that each precoding vector $\mathbf{p}_i = \sqrt{\alpha_i \mathcal{P}_B}\tilde{\mathbf{p}}$ with $\tilde{\mathbf{p}}$ being an arbitrary complex-valued unit-norm vector and $\alpha_{\mathbb{K}} + \sum_{m\in\mathbb{M}} \alpha_{\mathbb{K}_m} + \sum_{k\in\mathbb{K}} \alpha_k = 1$.

III. SINR FOR HRS

As per the 2L-HRS scheme, three different data streams (i.e., $x_{\mathbb{K}}$, $x_{\mathbb{K}_m}$, and x_k) need to be decoded by each NU and CEU. The decoding order is based on the order of the data streams, i.e., a higher order data stream is decoded prior to a lower order data stream.

A. CHARACTERIZATION OF SINR

Each user first decodes the K-order common data stream by considering the interference of all other data streams as noise. Therefore, the SINR for common data stream at q-th NU and k-th CEU can be obtained from (2) and (5), respectively, as

$$\gamma_{q,\mathbb{K}} = \frac{\alpha_{\mathbb{K}}\left|\mathbf{g}_q^{\mathrm{H}}\tilde{\mathbf{p}}\right|^2}{\sum_{i\in\mathbb{M}} \alpha_{\mathbb{K}_i}\left|\mathbf{g}_q^{\mathrm{H}}\tilde{\mathbf{p}}\right|^2 + \sum_{j\in\mathbb{K}} \alpha_j\left|\mathbf{g}_q^{\mathrm{H}}\tilde{\mathbf{p}}\right|^2 + \frac{1}{\rho_B}}, \tag{6}$$

$$\gamma_{k,\mathbb{K}} = \frac{\alpha_{\mathbb{K}}\left|\boldsymbol{\phi}_m^{\mathrm{H}}\mathbf{F}_{m,k}\tilde{\mathbf{h}}\right|^2}{\sum_{i\in\mathbb{M}} \alpha_{\mathbb{K}_i}\left|\boldsymbol{\phi}_m^{\mathrm{H}}\mathbf{F}_{m,k}\tilde{\mathbf{h}}\right|^2 + \sum_{j\in\mathbb{K}} \alpha_j\left|\boldsymbol{\phi}_m^{\mathrm{H}}\mathbf{F}_{m,k}\tilde{\mathbf{h}}\right|^2 + \frac{1}{\rho_B}}, \tag{7}$$

where $\tilde{\mathbf{h}} = \mathbf{H}_m\tilde{\mathbf{p}}$. On successful decoding of common data stream $x_{\mathbb{K}}$, its contribution is removed from the received signals y_q and y_k, respectively. Next, the m-th common-to-group data stream $x_{\mathbb{K}_m}$, $m \in \mathbb{M}$, is decoded by the all the users in group G_m by treating all other common-to-group data streams and all private data streams as noise. Therefore, the SINR for decoding K_0-order common-to-group data stream at q-th NU can be given as

$$\gamma_{q,\mathbb{K}_0} = \frac{\alpha_{\mathbb{K}_0}\left|\mathbf{g}_q^{\mathrm{H}}\tilde{\mathbf{p}}\right|^2}{\sum_{i\in\mathbb{M}'} \alpha_{\mathbb{K}_i}\left|\mathbf{g}_q^{\mathrm{H}}\tilde{\mathbf{p}}\right|^2 + \sum_{j\in\mathbb{K}} \alpha_j\left|\mathbf{g}_q^{\mathrm{H}}\tilde{\mathbf{p}}\right|^2 + \frac{1}{\rho_B}}. \tag{8}$$

Similarly, the SINR for decoding the K_m-order common-to-group data stream at k-th CEU, $k \in \mathbb{K}_m$, can be given as

$$\gamma_{k,\mathbb{K}_m} = \frac{\alpha_{\mathbb{K}_m}\left|\boldsymbol{\phi}_m^{\mathrm{H}}\mathbf{F}_{m,k}\tilde{\mathbf{h}}\right|^2}{\sum_{\substack{i\in\mathbb{M}\\ i\neq m}} \alpha_{\mathbb{K}_i}\left|\boldsymbol{\phi}_m^{\mathrm{H}}\mathbf{F}_{m,k}\tilde{\mathbf{h}}\right|^2 + \sum_{j\in\mathbb{K}} \alpha_j\left|\boldsymbol{\phi}_m^{\mathrm{H}}\mathbf{F}_{m,k}\tilde{\mathbf{h}}\right|^2 + \frac{1}{\rho_B}}. \tag{9}$$

In the end, each NU removes the contribution of the decoded common-to-group data stream from the received signal y_q and then decodes its own private data stream x_q. Thus, the SINR for decoding 1-order data stream x_q can be written as

$$\gamma_q = \frac{\alpha_q\left|\mathbf{g}_q^{\mathrm{H}}\tilde{\mathbf{p}}\right|^2}{\sum_{i\in\mathbb{M}'} \alpha_{\mathbb{K}_i}\left|\mathbf{g}_q^{\mathrm{H}}\tilde{\mathbf{p}}\right|^2 + \sum_{\substack{j\in\mathbb{K}\\ j\neq q}} \alpha_j\left|\mathbf{g}_q^{\mathrm{H}}\tilde{\mathbf{p}}\right|^2 + \frac{1}{\rho_B}}. \tag{10}$$

Similarly, the k-th CEU removes the contribution of the decoded common-to-group data stream from the received

signal y_k and decodes its own private data stream x_k. The SINR for decoding the private stream x_k can be written as

$$\gamma_k = \frac{\alpha_k \left|\boldsymbol{\phi}_m^{\mathrm{H}} \mathbf{F}_{m,k} \tilde{\mathbf{h}}\right|^2}{\sum_{\substack{i\in\mathbb{M}\\ i\neq m}} \alpha_{\mathbb{K}_i} \left|\boldsymbol{\phi}_m^{\mathrm{H}} \mathbf{F}_{m,k} \tilde{\mathbf{h}}\right|^2 + \sum_{\substack{j\in\mathbb{K}\\ j\neq k}} \alpha_j \left|\boldsymbol{\phi}_m^{\mathrm{H}} \mathbf{F}_{m,k} \tilde{\mathbf{h}}\right|^2 + \frac{1}{\rho_B}}. \tag{11}$$

It can be seen from (7), (9), and (11) that the choice of vector $\boldsymbol{\phi}_m$ is crucial for analyzing the system performance of CEUs in IRS-aided downlink network. There are different solutions available in the literature such as ideal or Zero Forcing (ZF) design, finite resolution-based design using discrete fourier transform (DFT), and cost-effective on-off control [22]. Due to the simplicity and scalability of the design (mainly for large reflecting elements) to configure and control the IRS, we consider on-off scheme in this work.

Note that the cell-edge users' effective channel vectors are determined by the choice of Φ_m (for $m = 1, 2, \ldots, M$), where $\varphi_{m,n}$ and $\beta_{m,n}(\varphi_{m,n})$, $n = 1, 2, \ldots, N_r$ are usually arbitrary. In literature [10], [12], [18], the choices for $\varphi_{m,n}$ and $\beta_{m,n}(\varphi_{m,n})$, $n = 1, 2, \ldots, N_r$ are usually arbitrary. However, due to the limitations on hardware of the IRS this assumption may not always hold true. Hence, in this paper we assume finite resolution beamforming through the ON-OFF control approach, whereby each diagonal element of Φ_m is either 1 (on) or 0 (off), like the one proposed in [22].

IV. PROPOSED ON-OFF SCHEME TO CONTROL IRS WITH PRACTICAL PHASE SHIFTS

In this section, we describe the proposed *On-Off* scheme to control IRSs with practical phase shifts. In this scheme, each reflecting element of IRS can either be OFF (i.e., inactive) or ON (i.e., active). For inactive elements, the reflection amplitude will be zero and for active elements, we consider a practical reflection amplitude[2] $\beta_n(\varphi_n)$ defined as [40]

$$\beta_n(\varphi_n) = (1 - \beta_{\min}) \left[\frac{1 + \sin(\varphi_n - \theta)}{2}\right]^{\epsilon} + \beta_{\min}, \tag{12}$$

where $\beta_{\min} \geq 0$ denotes the minimum reflection amplitude, $\theta \geq 0$ is the difference between $-\pi/2$ and the phase corresponding to $\beta_{\min}$, and ϵ is a positive constant related to the circuitry of the reflecting element. In order to have a finite resolution based design, we consider that the continuous phase φ_n is first quantized uniformly by utilizing a ν-bit quantizer to give a discrete phase shift value from $\mathcal{L} = 2^{\nu}$ discrete levels. Therefore, if $\varphi_n \sim U(-\pi, \pi)$, then the quantized phase shift value $\tilde{\varphi}_n \in \{-\pi + 0.5\Delta, -\pi + 1.5\Delta, \ldots, -\pi + 0.5(2L-1)\Delta\}$, where $\Delta = \frac{2\pi}{\mathcal{L}}$.

Let the number of reflecting elements at IRS is factored as $N_r = L_r D_r$, such that L_r and D_r are positive integers, then we define a $L_r \times N_r$ matrix $\mathbf{A}$ as

$$\mathbf{A} = \begin{bmatrix} \mathbf{u}_1 & \mathbf{0} & \mathbf{0} & \cdots & \mathbf{0} \\ \mathbf{0} & \mathbf{u}_2 & \mathbf{0} & \cdots & \mathbf{0} \\ \mathbf{0} & \mathbf{0} & \mathbf{u}_3 & \cdots & \mathbf{0} \\ \vdots & \vdots & \vdots & \ddots & \vdots \\ \mathbf{0} & \mathbf{0} & \mathbf{0} & \cdots & \mathbf{u}_{L_r} \end{bmatrix} \tag{13}$$

where $\mathbf{u}_\ell = \{\beta_j(\varphi_j)\}_{j=(\ell-1)D_r+1}^{\ell D_r}$, $\ell = 1, 2, \ldots, L_r$, represents a $1 \times D_r$ vector containing the practical reflection amplitudes of D_r active reflecting elements and $\mathbf{0}$ is the $1 \times D_r$ vector of all zeros. Let $\mathbf{a}_\ell$, $\ell = 1, 2, \ldots, L_r$, denotes the ℓ-th row vector of matrix $\mathbf{A}$, then we choose $\boldsymbol{\phi}^{\mathrm{H}} = \mathbf{a}_\ell$, such that $\mathbf{a}_\ell$ maximizes the SINRs in (15). Therefore, the optimum SINRs at the k-th user can be given as

$$\begin{aligned} \tilde{\gamma}_{k,\mathbb{K}} &\triangleq \max\left(\left\{\gamma_{k,\mathbb{K}}(\mathbf{a}_\ell)\right\}_{\ell=1}^{L_r}\right), \\ \tilde{\gamma}_{k,\mathbb{K}_m} &\triangleq \max\left(\left\{\gamma_{k,\mathbb{K}_m}(\mathbf{a}_\ell)\right\}_{\ell=1}^{L_r}\right), \\ \tilde{\gamma}_{k} &\triangleq \max\left(\left\{\gamma_{k}(\mathbf{a}_\ell)\right\}_{\ell=1}^{L_r}\right), \end{aligned} \tag{14}$$

where

$$\begin{aligned} \gamma_{k,\mathbb{K}}(\mathbf{a}_\ell) &= \frac{\alpha_{\mathbb{K}} \left|\mathbf{a}_\ell^{\mathrm{H}} \mathbf{F}_{m,k} \tilde{\mathbf{h}}\right|^2}{\sum_{i\in\mathbb{M}} \alpha_{\mathbb{K}_i} \left|\mathbf{a}_\ell^{\mathrm{H}} \mathbf{F}_{m,k} \tilde{\mathbf{h}}\right|^2 + \sum_{j\in\mathbb{K}} \alpha_j \left|\mathbf{a}_\ell^{\mathrm{H}} \mathbf{F}_{m,k} \tilde{\mathbf{h}}\right|^2 + \frac{1}{\rho_B}}, \\ \gamma_{k,\mathbb{K}_m}(\mathbf{a}_\ell) &= \frac{\alpha_{\mathbb{K}_m} \left|\mathbf{a}_\ell^{\mathrm{H}} \mathbf{F}_{m,k} \tilde{\mathbf{h}}\right|^2}{\sum_{\substack{i\in\mathbb{M}\\ i\neq m}} \alpha_{\mathbb{K}_i} \left|\mathbf{a}_\ell^{\mathrm{H}} \mathbf{F}_{m,k} \tilde{\mathbf{h}}\right|^2 + \sum_{j\in\mathbb{K}} \alpha_j \left|\mathbf{a}_\ell^{\mathrm{H}} \mathbf{F}_{m,k} \tilde{\mathbf{h}}\right|^2 + \frac{1}{\rho_B}}, \\ \gamma_{k}(\mathbf{a}_\ell) &= \frac{\alpha_{k} \left|\mathbf{a}_\ell^{\mathrm{H}} \mathbf{F}_{m,k} \tilde{\mathbf{h}}\right|^2}{\sum_{\substack{i\in\mathbb{M}\\ i\neq m}} \alpha_{\mathbb{K}_i} \left|\mathbf{a}_\ell^{\mathrm{H}} \mathbf{F}_{m,k} \tilde{\mathbf{h}}\right|^2 + \sum_{\substack{j\in\mathbb{K}\\ j\neq k}} \alpha_j \left|\mathbf{a}_\ell^{\mathrm{H}} \mathbf{F}_{m,k} \tilde{\mathbf{h}}\right|^2 + \frac{1}{\rho_B}}. \end{aligned} \tag{15}$$

Remark 1: It is worth noting that for a given ℓ, random SINRs $\gamma_{k,\mathbb{K}}(\mathbf{a}_\ell)$, $\gamma_{k,\mathbb{K}_m}(\mathbf{a}_\ell)$, and $\gamma_k(\mathbf{a}_\ell)$ (defined in (15)) are dependent on each other. However, the set of SINRs $\{\gamma_{k,\mathbb{K}}(\mathbf{a}_\ell), \gamma_{k,\mathbb{K}_m}(\mathbf{a}_\ell), \gamma_k(\mathbf{a}_\ell)\}$ is independent of another set $\{\gamma_{k,\mathbb{K}}(\mathbf{a}_\kappa), \gamma_{k,\mathbb{K}_m}(\mathbf{a}_\kappa), \gamma_k(\mathbf{a}_\kappa)\}$ for all $\kappa \neq \ell$, $\kappa, \ell = 1, 2, \ldots, L_r$. This implies that SINR $\gamma_{k,\mathbb{K}}(\mathbf{a}_\ell)$ is independent of $\gamma_{k,\mathbb{K}}(\mathbf{a}_\kappa)$, SINR $\gamma_{k,\mathbb{K}_m}(\mathbf{a}_\ell)$ is independent of $\gamma_{k,\mathbb{K}_m}(\mathbf{a}_\kappa)$, and SINR $\gamma_k(\mathbf{a}_\ell)$ is independent of $\gamma_k(\mathbf{a}_\kappa)$ for all $\kappa \neq \ell$. Further, the Monte Carlo simulations verify that maximum values of three SINRs, i.e., $\tilde{\gamma}_{k,\mathbb{K}}$, $\tilde{\gamma}_{k,\mathbb{K}_m}$, and $\tilde{\gamma}_k$ are obtained at same $\mathbf{a}_\ell$. In other words, if a particular choice of $\boldsymbol{\phi}_m$ (i.e., a particular active reflecting element pattern) maximizes the K-order common message SINR, then the same $\boldsymbol{\phi}_m$ also maximizes both the K_m-order common-to-group SINR and unity order private message SINR.

V. OUTAGE ANALYSIS OF IRS-AIDED HRS

A. OUTAGE PROBABILITY FOR CEU

Under 2L-HRS scheme, a CEU will said to be in outage if and only if the three optimum SINRs (defined in (14)) corresponding to common-to-all, common-to-group, and private

2. For simplicity, we skip the subscript 'm' corresponding to m-th IRS. The discussion in this section is valid for any arbitrary IRS among the considered IRSs.

messages simultaneously fall below the respective threshold SINRs. Thus, the outage probability at k-th user can be defined as,

$$\mathbb{P}_k^{\text{OUT}} \triangleq \Pr\{\tilde{\gamma}_{k,\mathbb{K}} < \tau_{\mathbb{K}}, \tilde{\gamma}_{k,\mathbb{K}_m} < \tau_{\mathbb{K}_m}, \tilde{\gamma}_k < \tau_0\}, \quad (16)$$

where $\tau_{\mathbb{K}}, \tau_{\mathbb{K}_m}$, and τ_0 are threshold SINRs for common-to-all, common-to-group, and private messages, respectively. $\Pr\{\cdot,\cdot,\cdot\}$ represents the joint probability. Following [41], we can write (16) as,

$$\begin{aligned}\mathbb{P}_k^{\text{OUT}} &= \mathbb{F}_{\tilde{\gamma}_{k,\mathbb{K}}}(\tau_{\mathbb{K}}) + \mathbb{F}_{\tilde{\gamma}_{k,\mathbb{K}_m}}(\tau_{\mathbb{K}_m}) + \mathbb{F}_{\tilde{\gamma}_k}(\tau_0) \\ &\quad - \mathbb{F}_{\tilde{\gamma}_{k,\mathbb{K}},\tilde{\gamma}_{k,\mathbb{K}_m}}(\tau_{\mathbb{K}}, \tau_{\mathbb{K}_m}) - \mathbb{F}_{\tilde{\gamma}_{k,\mathbb{K}},\tilde{\gamma}_k}(\tau_{\mathbb{K}}, \tau_0) \\ &\quad - \mathbb{F}_{\tilde{\gamma}_{k,\mathbb{K}_m},\tilde{\gamma}_k}(\tau_{\mathbb{K}_m}, \tau_0) + \mathbb{F}_{\tilde{\gamma}_{k,\mathbb{K}},\tilde{\gamma}_{k,\mathbb{K}_m},\tilde{\gamma}_k}(\tau_{\mathbb{K}}, \tau_{\mathbb{K}_m}, \tau_0),\end{aligned} \quad (17)$$

where $\mathbb{F}_{X_1}(\cdot)$ denotes the cumulative distribution function (CDF) of a RV X_1, $\mathbb{F}_{X_1,X_2}(\cdot,\cdot)$ and $\mathbb{F}_{X_1,X_2,X_3}(\cdot,\cdot,\cdot)$ are the joint CDFs of two and three RVs, respectively. If we define a set $X \equiv \{\gamma_{k,\mathbb{K}}, \gamma_{k,\mathbb{K}_m}, \gamma_k\}$, then for all $X_1, X_2, X_3 \in X$ and $\tilde{X}_j \triangleq \max(\{X_j(\mathbf{a}_\ell)\}_{\ell=1}^{L_r})$, $j = 1, 2, 3$, following can be written using the discussion in Remark 1,

$$\begin{aligned}\mathbb{F}_{\tilde{X}_1}(\tau_1) &= \prod_{\ell=1}^{L_r} \mathbb{F}_{X_1(\mathbf{a}_\ell)}(\tau_1), \\ \mathbb{F}_{\tilde{X}_1,\tilde{X}_2}(\tau_1, \tau_2) &= \prod_{\ell=1}^{L_r} \mathbb{F}_{X_1(\mathbf{a}_\ell),X_2(\mathbf{a}_\ell)}(\tau_1, \tau_2), \\ \mathbb{F}_{\tilde{X}_1,\tilde{X}_2,\tilde{X}_3}(\tau_1, \tau_2, \tau_3) &= \prod_{\ell=1}^{L_r} \mathbb{F}_{X_1(\mathbf{a}_\ell),X_2(\mathbf{a}_\ell),X_3(\mathbf{a}_\ell)}(\tau_1, \tau_2, \tau_3),\end{aligned} \quad (18)$$

where $\tau_1, \tau_2, \tau_3 \in T$, with $T \equiv \{\tau_{\mathbb{K}}, \tau_{\mathbb{K}_m}, \tau_0\}$. It is clear from Remark 1 that the set of random variables $\{X_1(\mathbf{a}_\ell), X_2(\mathbf{a}_\ell), X_3(\mathbf{a}_\ell)\}$ is independent of another set $\{X_1(\mathbf{a}_\kappa), X_2(\mathbf{a}_\kappa), X_3(\mathbf{a}_\kappa)\}$ for all $\kappa \neq \ell$, $\kappa, \ell = 1, 2, \ldots, L_r$. This also implies that random variable $X_1(\mathbf{a}_\ell)$ is independent of $X_1(\mathbf{a}_\kappa)$, $X_2(\mathbf{a}_\ell)$ is independent of $X_2(\mathbf{a}_\kappa)$, and $X_3(\mathbf{a}_\ell)$ is independent of $X_3(\mathbf{a}_\kappa)$ for all $\kappa \neq \ell$. Hence, the CDF of the maximum of L_r independent random variables (or set of random variables) can be written as the product of their marginal (or joint) CDFs.

Lemma 1: If $\mathbf{D}$ is a $P \times P$ diagonal matrix defined as $\mathbf{D} = \text{Diag}(d_1, d_2, \ldots, d_P)$ with element $d_p \sim \mathcal{CN}(0, \delta_d^2)$ and $\mathbf{b} = [b_1, b_2, \ldots, b_P]^{\text{T}}$ is a $P \times 1$ complex random vector such that $b_p \sim \mathcal{CN}(0, \delta_b^2)$, for $p = 1, 2, \ldots, P$, then for any arbitrary real-valued vector $\mathbf{c} = [c_1, c_2, \ldots, c_P]^{\text{T}}$ with $c_p \in (0, 1)$, the CDF of $W = |\mathbf{c}^{\text{H}}\mathbf{D}\mathbf{b}|^2$ can be given as

$$\mathbb{F}_W(w) = \sum_{j=1}^{J}\left(\prod_{\substack{i=1\\ i\neq j}}^{J} \frac{\lambda_i}{\lambda_i - \lambda_j}\right)\left[1 - 2\sqrt{w\lambda_j}K_{-1}\left(2\sqrt{w\lambda_j}\right)\right]. \quad (19)$$

where $K_v(\cdot)$ is the v-th order modified Bessel's function of second kind, $\lambda_j = \frac{1}{\delta_d^2\delta_b^2\tilde{c}_j^2}$, and $\tilde{c}_j$, $j = 1, 2, \ldots, J$, is a non-zero element of vector $\mathbf{c}$.

Proof: Let vector $\mathbf{c}$ contains J ($J \leq P$) non-zero elements $\tilde{c}_j$, $j \in \{1, 2, \ldots, J\}$, then we can define a RV U as

$$U = \mathbf{c}^{\text{H}}\mathbf{D}\mathbf{b} = \sum_{j=1}^{J} \tilde{c}_j d_j b_j. \quad (20)$$

Assuming that random vector $\mathbf{b}$ is known, we can write that $U|_{\mathbf{b}} \sim \mathcal{CN}(0, V)$ and $W|_{\mathbf{b}} \triangleq |U|^2|_{\mathbf{b}} \sim \text{Exp}(\frac{1}{V})$, where

$$V = \delta_d^2 \sum_{j=1}^{J} \tilde{c}_j^2 |b_j|^2 \triangleq \sum_{j=1}^{J} v_j. \quad (21)$$

The $\text{Exp}(\lambda)$ represents the exponential distribution with rate parameter λ. Since $b_j \sim \mathcal{CN}(0, \delta_b^2)$, it follows that $v_j = \delta_d^2\tilde{c}_j^2|b_j|^2 \sim \text{Exp}(\lambda_j)$, $j = 1, 2, \ldots, J$, with $\lambda_j = \frac{1}{\delta_d^2\delta_b^2\tilde{c}_j^2}$. Since the sum of J i.n.i.d. exponential RVs follows Hypoexponential distribution [42], we can get the probability density function (PDF) of V as

$$f_V(v) = \sum_{j=1}^{J} \lambda_j e^{-v\lambda_j}\left(\prod_{\substack{i=1\\ i\neq j}}^{J} \frac{\lambda_i}{\lambda_i - \lambda_j}\right), \quad v \geq 0. \quad (22)$$

Now, we can obtain the PDF of W by using (22) in $f_W(w) = \int_0^\infty \frac{1}{v} e^{-\frac{w}{v}} f_V(v)\, dv$ followed by the use of [43, eq. (3.471.9)] as

$$f_W(w) = \sum_{j=1}^{J} 2\lambda_j\left(\prod_{\substack{i=1\\ i\neq j}}^{J} \frac{\lambda_i}{\lambda_i - \lambda_j}\right) K_0\left(2\sqrt{w\lambda_j}\right), \quad (23)$$

and by substituting (23) in $\mathbb{F}_W(w) = \int_0^w f_W(x)\, dx$ along with the use of [43, eq. (6.561.12)], we get (19). ∎

Corollary 1: For J=1 (special case), i.e., vector $\mathbf{c}$ contains only one non-zero element (say $\tilde{c}$), the CDF of $W = |\mathbf{c}^{\text{H}}\mathbf{D}\mathbf{b}|^2$ can be given as

$$\mathbb{F}_W(w) = \left[1 - 2\sqrt{w\tilde{\lambda}}K_{-1}\left(2\sqrt{w\tilde{\lambda}}\right)\right], \quad (24)$$

where $\tilde{\lambda} = \frac{1}{\delta_d^2\delta_b^2\tilde{c}^2}$.

Corollary 2: If $\lambda_j = \lambda$ for all $j = 1, 2, \ldots, J$, i.e., all the non-zero elements of vector $\mathbf{c}$ are equal, then the random variable V (defined in (21)) will follow Chi-Square distribution with $2J$ degrees of freedom. Thus, the PDF and CDF of $W = |\mathbf{c}^{\text{H}}\mathbf{D}\mathbf{b}|^2$ in this case can be given as

$$f_W(w) = \frac{2\lambda^{\frac{J+1}{2}}}{\Gamma(J)} w^{\frac{J-1}{2}} K_{J-1}\left(2\sqrt{w\lambda}\right), \quad (25)$$

$$\mathbb{F}_W(w) = 1 - \frac{2\lambda^{\frac{J}{2}}}{\Gamma(J)} w^{\frac{J}{2}} K_J\left(2\sqrt{w\lambda}\right). \quad (26)$$

where (25) and (26) are obtained by utilizing [43, eq. (3.471.9)] and [43, eq. (6.561.12)], respectively.

If we define $|\mathbf{a}_\ell^{\text{H}}\mathbf{F}_{m,k}\tilde{\mathbf{h}}|^2 \triangleq W_\ell$, then the CDF of RV W_ℓ can be directly obtained from (19) by substituting $J = D_r$ and $\lambda_j = \frac{1}{\Omega_h\Omega_f\beta_j^2(\varphi_j)}$, $j = 1, 2, \ldots, D_r$ and $D_r \geq 2$. Therefore,

the marginal CDF of SINR $X_1(\mathbf{a}_\ell)$, where $X_1 \in X$, $X \equiv \{\gamma_{k,\mathbb{K}}, \gamma_{k,\mathbb{K}_m}, \gamma_k\}$ can be evaluated as

$$\mathbb{F}_{X_1(\mathbf{a}_\ell)}(\tau_1) = \sum_{j=1}^{D_r}\left(\prod_{\substack{i=1\\ i\neq j}}^{D_r}\frac{\lambda_i}{\lambda_i-\lambda_j}\right) \times\left[1-2\sqrt{\frac{\tau_1\lambda_j}{\rho_B\eta_1}}K_{-1}\left(2\sqrt{\frac{\tau_1\lambda_j}{\rho_B\eta_1}}\right)\right], \quad (27)$$

where the parameters (τ_1, η_1) are chosen as an element of a set $\mathcal{T}_m \equiv \{(\tau_{\mathbb{K}}, \eta_{\mathbb{K}}), (\tau_{\mathbb{K}_m}, \eta_{\mathbb{K}_m}), (\tau_0, \eta_0)\}$ with

$$\begin{aligned}\eta_{\mathbb{K}} &= \alpha_{\mathbb{K}} - \tau_{\mathbb{K}}\sum_{i\in\mathbb{M}}\alpha_{\mathbb{K}_i} - \tau_{\mathbb{K}}\sum_{j\in\mathbb{K}}\alpha_j,\\ \eta_{\mathbb{K}_m} &= \alpha_{\mathbb{K}_m} - \tau_{\mathbb{K}_m}\sum_{\substack{i\in\mathbb{M}\\ i\neq m}}\alpha_{\mathbb{K}_i} - \tau_{\mathbb{K}_m}\sum_{j\in\mathbb{K}}\alpha_j,\\ \eta_0 &= \alpha_k - \tau_0\sum_{\substack{i\in\mathbb{M}\\ i\neq m}}\alpha_{\mathbb{K}_i} - \tau_0\sum_{\substack{j\in\mathbb{K}\\ j\neq k}}\alpha_j. \end{aligned} \quad (28)$$

Similarly, we can obtain the joint CDF of $X_1(\mathbf{a}_\ell), X_2(\mathbf{a}_\ell)$, where $X_1, X_2 \in X$, as

$$\mathbb{F}_{X_1(\mathbf{a}_\ell),X_2(\mathbf{a}_\ell)}(\tau_1,\tau_2) = \sum_{j=1}^{D_r}\left(\prod_{\substack{i=1\\ i\neq j}}^{D_r}\frac{\lambda_i}{\lambda_i-\lambda_j}\right) \times\left[1-2\sqrt{\frac{\xi_1\lambda_j}{\rho_B}}K_{-1}\left(2\sqrt{\frac{\xi_1\lambda_j}{\rho_B}}\right)\right], \quad (29)$$

where $\xi_1 = \min(\frac{\tau_1}{\eta_1}, \frac{\tau_2}{\eta_2})$ and the parameters $(\tau_1, \eta_1), (\tau_2, \eta_2) \in \mathcal{T}_m$ with $(\tau_1, \eta_1) \neq (\tau_2, \eta_2)$. Finally, we may evaluate the joint CDF of three SINRs (defined in (15)) as

$$\begin{aligned}&\mathbb{F}_{X_1(\mathbf{a}_\ell),X_2(\mathbf{a}_\ell),X_3(\mathbf{a}_\ell)}(\tau_1,\tau_2,\tau_3)\\ &= \sum_{j=1}^{D_r}\left(\prod_{\substack{i=1\\ i\neq j}}^{D_r}\frac{\lambda_i}{\lambda_i-\lambda_j}\right) \times\left[1-2\sqrt{\frac{\xi_2\lambda_j}{\rho_B}}K_{-1}\left(2\sqrt{\frac{\xi_2\lambda_j}{\rho_B}}\right)\right], \end{aligned} \quad (30)$$

where $\xi_2 = \min(\frac{\tau_1}{\eta_1}, \frac{\tau_2}{\eta_2}, \frac{\tau_3}{\eta_3})$ with $\tau_1, \tau_2, \tau_3 \in T$ and $\eta_{\mathbb{K}}, \eta_{\mathbb{K}_m}$, and η_0 given in (28). Utilizing (27)-(30) along with (18) in (17), we obtain the closed-form expression for outage probability of k-th cell-edge user. It should be noted that for $D_r = 1$, (24) can be utilized for evaluating the marginal and joint CDFs of three SINRs.

Observation 1: For real and positive threshold SINRs for common-to-all, common-to-group, and private messages (i.e., $\tau_{\mathbb{K}}, \tau_{\mathbb{K}_m}, \tau_k > 0$), it can be observed by using (28) in (27) that the three power allocation coefficients must satisfy the following conditions as

$$\alpha_{\mathbb{K}} > \frac{\tau_{\mathbb{K}}}{1+\tau_{\mathbb{K}}}, \quad \alpha_{\mathbb{K}_m} > \frac{\tau_{\mathbb{K}_m}(1-\alpha_{\mathbb{K}})}{1+\tau_{\mathbb{K}_m}},$$

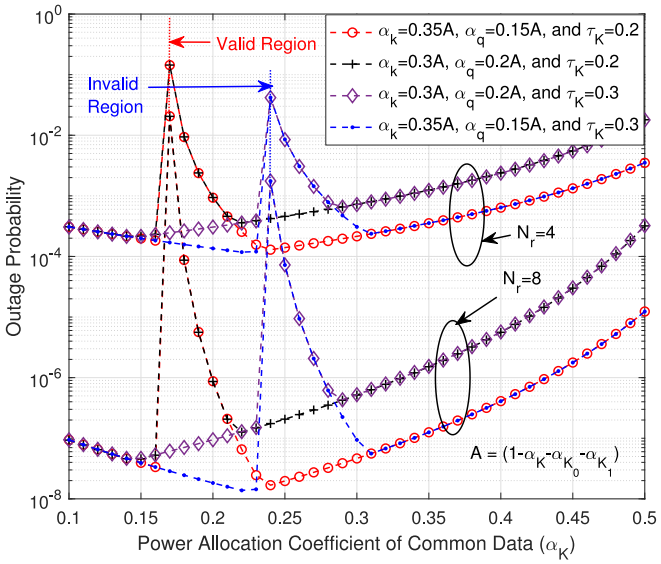

FIGURE 2. Outage performance of CEU with varying $\alpha_{\mathbb{K}}$ for $K = 4$ and $\rho_B = 20$ dB.

$$\text{and } \alpha_k > \frac{\tau_k(1-\alpha_{\mathbb{K}}-\alpha_{\mathbb{K}_m})}{1+\tau_k}, \quad (31)$$

such that $\eta_{\mathbb{K}}, \eta_{\mathbb{K}_m}, \eta_k > 0$. The optimum values of these power allocation coefficients are chosen so as to minimize the outage probability. In Fig. 2, Fig. 3, and Fig. 4, we have shown the outage probability variations of a CEU for varying $\alpha_{\mathbb{K}}$, $\alpha_{\mathbb{K}_m}$, and α_k, respectively, under 4-user scenario with equal NUs and CEUs. For Fig. 2, we have considered $\tau_{\mathbb{K}} = 0.2, 0.3$ with $\tau_{\mathbb{K}_m} = \tau_k = 0.2$ and $\rho_B = 20$ dB. Furthermore, we consider $\alpha_{\mathbb{K}_1} = 2\alpha_{\mathbb{K}_0} = 0.2$ and remaining power is divided in four private messages as (i) each CEU and NU getting 35% and 15% of the power available for private messages, i.e., $\alpha_k = 0.35(1 - \alpha_{\mathbb{K}} - \alpha_{\mathbb{K}_0} - \alpha_{\mathbb{K}_1})$, and (ii) each CEU and NU getting 30% and 20% of the power available for private messages, i.e., $\alpha_k = 0.3(1 - \alpha_{\mathbb{K}} - \alpha_{\mathbb{K}_0} - \alpha_{\mathbb{K}_1})$. Under these settings, it can be observed from Fig. 2 that the valid range for $\alpha_{\mathbb{K}}$ with $N_r = 4, 8$ both is $\alpha_{\mathbb{K}} > 0.17$ for $\tau_{\mathbb{K}} = 0.2$ and $\alpha_{\mathbb{K}} > 0.24$ for $\tau_{\mathbb{K}} = 0.3$, which is inline with (31). Moreover, the outage probability is minimized at $\alpha_{\mathbb{K}} \approx 0.24, 0.22$ for scenario (i) and (ii) given above, respectively with $\tau_{\mathbb{K}} = 0.2$. However, if we have increase the threshold SINR of common-to-all message to 0.3, we observe an increase in the optimum value of $\alpha_{\mathbb{K}}$ under both power allocation scenarios.

In Fig. 3, we have used the optimum values of $\alpha_{\mathbb{K}}$ to observe the variations of outage probability with power allocation coefficient of common-to-group data. We have also fixed $\rho_B = 20$ dB, $\tau_{\mathbb{K}} = \tau_{\mathbb{K}_m} = \tau_k = 0.2$, and $\alpha_{\mathbb{K}_0} = 0.5\alpha_{\mathbb{K}_1}$. It can be noticed from Fig. 3 that for a group of 2 CEUs having 30% of total private messages power each, $0.13 < \alpha_{\mathbb{K}_1} < 0.35$, and CEU outage probability is minimized at $\alpha_{\mathbb{K}_1} \approx 0.18$. Similarly, if we allocate 35% of total private messages power to each CEU, we get $0.13 < \alpha_{\mathbb{K}_1} < 0.38$, and the minimum occurs at

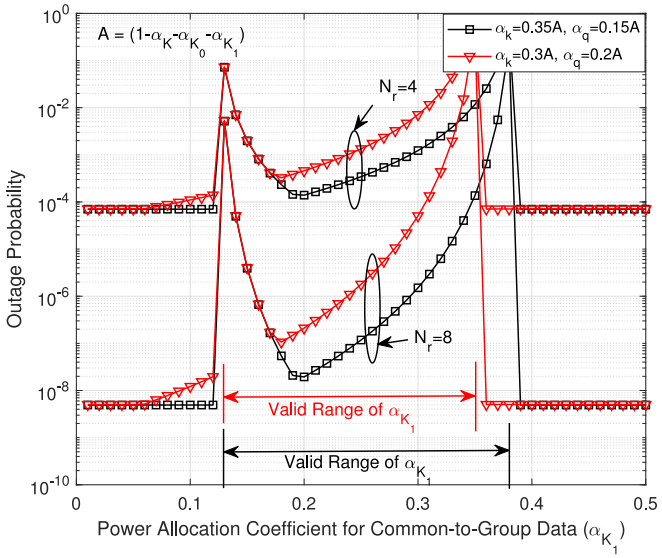

FIGURE 3. Outage performance of CEU with varying $\alpha_{\mathbb{K}_1}$ for $K = 4$ and $\rho_B = 20$ dB.

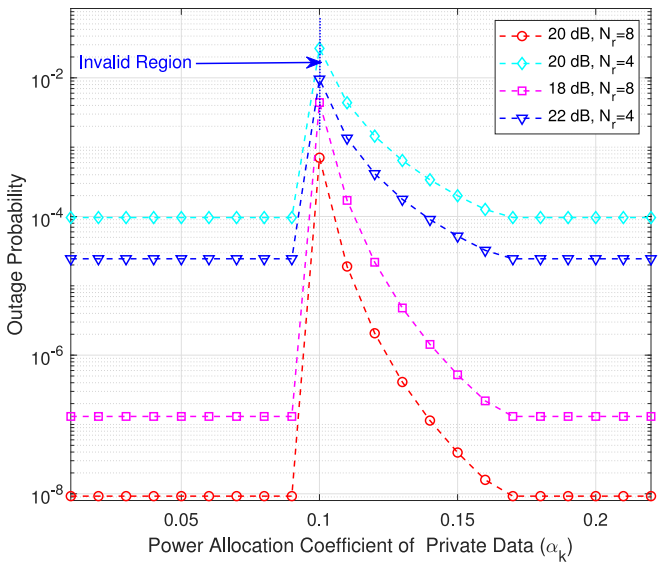

FIGURE 4. Outage performance of CEU with varying α_k for $K = 4$.

$\alpha_{\mathbb{K}_1} \approx 0.2$. In the end, we have optimized the outage probability for the power allocation coefficient for private message of the CEU (i.e., α_k, $k \in \mathbb{K}_1$) in Fig. 4. We have taken $\alpha_{\mathbb{K}} = 0.25, \alpha_{\mathbb{K}_0} = 0.1$ and $\alpha_{\mathbb{K}_1} = 0.2$ in Fig. 4. Furthermore, we have assumed that all the users in a group are allocated with equal power. It can be seen from Fig. 4 that for all values of ρ_B and N_r considered in the figure, the outage probability is minimum for $\alpha_k > 0.16$, which is approximately 35% of $(1 - \alpha_{\mathbb{K}} - \alpha_{\mathbb{K}_0} - \alpha_{\mathbb{K}_1})$, i.e., fraction of available power for all private messages.

In the numerical results section, the optimum values of power allocation coefficients (for given threshold SINRs of common-to-all, common-to-group, and private data) are chosen in accordance to Observation 2.

B. ASYMPTOTIC OUTAGE OF CEU FOR LARGE N_r

In order to find the further insights, we investigate the outage behavior of a CEU for sufficiently large number of reflecting elements, i.e., $N_r \to \infty$. For this, we assume the ideal phase shift scenario (i.e., $\beta_{\min} = 1$) at each reflecting element of IRS. Therefore, $\beta_n(\varphi_n) = 1$ for all n and $\lambda_j = \frac{1}{\Omega_h \Omega_f} = \lambda$, for all j. Following the results in Corollary 2, we can write the CDF in (27) as

$$\mathbb{F}_{X_1(\mathbf{a}_\ell)}(\tau_1) = 1 - \frac{2}{\Gamma(D_r)} \left(\frac{\tau_1 \lambda}{\rho_B \eta_1} \right)^{\frac{D_r}{2}} K_{D_r} \left(2 \left(\frac{\tau_1 \lambda}{\rho_B \eta_1} \right)^{\frac{1}{2}} \right), \quad (32)$$

where $(\tau_1, \eta_1) \in \mathcal{T}_m$. Under ideal reflection conditions, $X_1(\mathbf{a}_\ell)$ will have equal average statistics due to the fact that $\mathbf{u}_\ell = \mathbf{1}_{1 \times D_r}$ for $\ell = 1, 2, \ldots L_r$. Thus, the CDF of $\tilde{X}_1$ (given in (18)) can be written as

$$\mathbb{F}_{\tilde{X}_1}(\tau_1) = \left[1 - \frac{2}{\Gamma(D_r)} \left(\frac{\tau_1 \lambda}{\rho_B \eta_1} \right)^{\frac{D_r}{2}} K_{D_r} \left(2 \left(\frac{\tau_1 \lambda}{\rho_B \eta_1} \right)^{\frac{1}{2}} \right) \right]^{L_r}. \quad (33)$$

For sufficiently large number of reflecting elements (i.e., $N_r \to \infty$), we have $L_r \to \infty$ for a fixed D_r. Using the relation $\lim_{n \to \infty} (1 - x)^n \approx e^{-nx}$ with some algebra, we can write the asymptotic CDF of $\tilde{X}_1$ as

$$\begin{aligned} \mathcal{F}_{\tilde{X}_1}(\tau_1) &= \lim_{N_r \to \infty} \mathbb{F}_{\tilde{X}_1}(\tau_1) \\ &= \exp\left\{ -\frac{2N_r}{\Gamma(D_r + 1)} \left(\frac{\tau_1 \lambda}{\rho_B \eta_1} \right)^{\frac{D_r}{2}} K_{D_r} \left(2 \left(\frac{\tau_1 \lambda}{\rho_B \eta_1} \right)^{\frac{1}{2}} \right) \right\}. \end{aligned} \quad (34)$$

In a similar fashion, we obtain the asymptotic expressions of joint CDFs (defined in (18)) as

$$\begin{aligned} &\mathcal{F}_{\tilde{X}_1, \tilde{X}_2}(\tau_1, \tau_2) \\ &\quad = \lim_{N_r \to \infty} \mathbb{F}_{\tilde{X}_1, \tilde{X}_2}(\tau_1, \tau_2) \\ &\quad = \exp\left\{ -\frac{2N_r}{\Gamma(D_r + 1)} \left(\frac{\xi_1 \lambda}{\rho_B} \right)^{\frac{D_r}{2}} K_{D_r} \left(2 \left(\frac{\xi_1 \lambda}{\rho_B} \right)^{\frac{1}{2}} \right) \right\}. \end{aligned} \quad (35)$$

and

$$\begin{aligned} &\mathcal{F}_{\tilde{X}_1, \tilde{X}_2, \tilde{X}_3}(\tau_1, \tau_2, \tau_3) \\ &\quad = \lim_{N_r \to \infty} \mathbb{F}_{\tilde{X}_1, \tilde{X}_2, \tilde{X}_3}(\tau_1, \tau_2, \tau_3) \\ &\quad = \exp\left\{ -\frac{2N_r}{\Gamma(D_r + 1)} \left(\frac{\xi_2 \lambda}{\rho_B} \right)^{\frac{D_r}{2}} K_{D_r} \left(2 \left(\frac{\xi_2 \lambda}{\rho_B} \right)^{\frac{1}{2}} \right) \right\}. \end{aligned} \quad (36)$$

Utilizing these asymptotic expressions of marginal and joint CDFs from (34)-(36) in (17), we get the asymptotic outage probability of k-th CEU for $N_r \to \infty$ as

$$\begin{aligned} \mathcal{P}_k^{\text{OUT}} &= \lim_{N_r \to \infty} \mathbb{P}_k^{\text{OUT}} \\ &= \mathcal{F}_{\tilde{\gamma}_{k,\mathbb{K}}}(\tau_{\mathbb{K}}) + \mathcal{F}_{\tilde{\gamma}_{k,\mathbb{K}_m}}(\tau_{\mathbb{K}_m}) + \mathcal{F}_{\tilde{\gamma}_k}(\tau_0) \\ &\quad - \mathcal{F}_{\tilde{\gamma}_{k,\mathbb{K}}, \tilde{\gamma}_{k,\mathbb{K}_m}}(\tau_{\mathbb{K}}, \tau_{\mathbb{K}_m}) - \mathcal{F}_{\tilde{\gamma}_{k,\mathbb{K}}, \tilde{\gamma}_k}(\tau_{\mathbb{K}}, \tau_0) \end{aligned}$$

$$- \mathcal{F}_{\tilde{\gamma}_{k,\mathbb{K}_m},\tilde{\gamma}_k}\left(\tau_{\mathbb{K}_m}, \tau_0\right) + \mathcal{F}_{\tilde{\gamma}_{k,\mathbb{K}},\tilde{\gamma}_{k,\mathbb{K}_m},\tilde{\gamma}_k}\left(\tau_{\mathbb{K}}, \tau_{\mathbb{K}_m}, \tau_0\right), \tag{37}$$

Further, we define a metric called *Log-Asymptotic Outage Order* ($\mathcal{O}_{N_r}$), which is the parameter associated with large values of reflecting elements (N_r), as the negative of the ratio of natural logarithm of asymptotic outage probability (for large N_r) and number of reflecting elements, i.e.,

$$\mathcal{O}_{N_r}^k = -\frac{\ln \mathcal{P}_k^{\text{OUT}}}{N_r}, \tag{38}$$

where $\mathcal{P}_k^{\text{OUT}}$ is given in (37). It is analogus to the diversity order which is obtained at high SNR values. This depicts the rate of variations of outage probability at high values of N_r. It explains about how quickly or slowly the outage probability is varying with respect to transmit power (or transmit SNR) under the assumptions of large reflecting surfaces. The insights obtained from the Log-Asymptotic Outage Order are discussed in the numerical results section.

C. DIVERSITY ORDER ANALYSIS

Further, we analyze the outage behavior of a CEU for high transmit power conditions, i.e., $\rho_B \to \infty$. Assuming the ideal phase shift scenario at IRS as considered in previous Subsection and following Corollary 2, we can write the joint CDF in (30) as

$$\mathbb{F}_{X_1(\mathbf{a}_\ell),X_2(\mathbf{a}_\ell),X_3(\mathbf{a}_\ell)}(\tau_1, \tau_2, \tau_3) = 1 - \frac{2}{\Gamma(D_r)}\left(\frac{\xi_2\lambda}{\rho_B}\right)^{\frac{D_r}{2}} \times K_{D_r}\left(2\left(\frac{\xi_2\lambda}{\rho_B}\right)^{\frac{D_r}{2}}\right), \tag{39}$$

Lemma 2: For high transmit power conditions, i.e., $\rho_B \to \infty$, and a given reflection coefficient vector $\boldsymbol{\phi}^{\text{H}} = \mathbf{a}_\ell$, the jont CDF in (39) can be approximated as

$$\lim_{\rho_B\to\infty} \mathbb{F}_{X_1(\mathbf{a}_\ell),X_2(\mathbf{a}_\ell),X_3(\mathbf{a}_\ell)}(\tau_1, \tau_2, \tau_3) = \begin{cases} \frac{\xi_2\lambda}{\rho_B}\ln\left(\frac{\rho_B}{\xi_2\lambda}\right), & \text{For } D_r = 1, \\ \frac{\xi_2\lambda}{\rho_B(D_r-1)}, & \text{For } D_r > 1. \end{cases} \tag{40}$$

Proof: As $\rho_B \to \infty$, the argument of the modified Bessel's function in (39) tends to zero. Following [43], we utilize two different approximations of $K_D(x)$ for $x \to 0$ as $K_1(x) \approx x^{-1} + 0.5x\ln(0.5x)$ and $K_D(x) \approx 0.5\{(2x^{-1})^D\Gamma(D) - (2x^{-1})^{D-2}\Gamma(D-1)\}$ for $D > 1$. Using these asymptotic values in (39), we get (40). ■

Corollary 3: By applying the L'Hôpital's rule in (40), we can show that for all values of D_r with $\rho_B \to \infty$,

$$\lim_{\rho_B\to\infty} \mathbb{F}_{X_1(\mathbf{a}_\ell),X_2(\mathbf{a}_\ell),X_3(\mathbf{a}_\ell)}(\tau_1, \tau_2, \tau_3) \propto \frac{1}{\rho_B}. \tag{41}$$

Following Lemma 2 along with the assumptions of ideal reflecting conditions, we can also write the following:

$$\lim_{\rho_B\to\infty} \mathbb{F}_{X_1(\mathbf{a}_\ell)}(\tau_1) = \begin{cases} \frac{\tau_1\lambda}{\rho_B\eta_1}\ln\left(\frac{\rho_B\eta_1}{\tau_1\lambda}\right), & \text{For } D_r = 1, \\ \frac{\tau_1\lambda}{\rho_B\eta_1(D_r-1)}, & \text{For } D_r > 1. \end{cases} \tag{42}$$

and

$$\lim_{\rho_B\to\infty} \mathbb{F}_{X_1(\mathbf{a}_\ell),X_2(\mathbf{a}_\ell)}(\tau_1, \tau_2) = \begin{cases} \frac{\xi_1\lambda}{\rho_B}\ln\left(\frac{\rho_B}{\xi_1\lambda}\right), & \text{For } D_r = 1, \\ \frac{\xi_1\lambda}{\rho_B(D_r-1)}, & \text{For } D_r > 1. \end{cases} \tag{43}$$

Remark 2: Utilizing (42) and (43) along with the result of Corollary 1 in (17), it can be deduced that for high transmit SNR conditions, the outage probability of the considered IRS-assisted downlink network with 2L-HRS using one-bit control achieves a diversity order of L_r, i.e.,

$$\lim_{\rho_B\to\infty} \mathbb{P}_k^{\text{OUT}} \propto \frac{1}{\rho_B^{L_r}}. \tag{44}$$

D. OUTAGE PROBABILITY FOR NU

The outage probability for q-th NU, $q \in \mathbb{K}_0$, can be defined as the probability of all the three SINRs at q-th NU (i.e., $\gamma_{q,\mathbb{K}}$, $\gamma_{q,\mathbb{K}_0}$, and γ_q) falling below the corresponding threshold SINRs and can be evaluated as

$$\mathbb{P}_q^{\text{OUT}} \triangleq \Pr\left\{\gamma_{q,\mathbb{K}} < \tau_{\mathbb{K}}, \gamma_{q,\mathbb{K}_0} < \tau_{\mathbb{K}_0}, \gamma_q < \tau_0\right\}, \tag{45}$$

which can further be written (similar to (17)) as

$$\begin{aligned}\mathbb{P}_q^{\text{OUT}} = {} & \mathbb{F}_{\gamma_{q,\mathbb{K}}}(\tau_{\mathbb{K}}) + \mathbb{F}_{\gamma_{q,\mathbb{K}_0}}\left(\tau_{\mathbb{K}_0}\right) + \mathbb{F}_{\gamma_q}(\tau_0) \\ & - \mathbb{F}_{\gamma_{q,\mathbb{K}},\gamma_{q,\mathbb{K}_0}}\left(\tau_{\mathbb{K}}, \tau_{\mathbb{K}_0}\right) - \mathbb{F}_{\gamma_{q,\mathbb{K}},\gamma_q}(\tau_{\mathbb{K}}, \tau_0) \\ & - \mathbb{F}_{\gamma_{q,\mathbb{K}_0},\gamma_q}\left(\tau_{\mathbb{K}_0}, \tau_0\right) + \mathbb{F}_{\gamma_{q,\mathbb{K}},\gamma_{q,\mathbb{K}_0},\gamma_q}\left(\tau_{\mathbb{K}}, \tau_{\mathbb{K}_0}, \tau_0\right).\end{aligned} \tag{46}$$

Since $\mathbf{g}_q \sim \mathcal{CN}(0, \Omega_g\mathbf{I})$, we may write $|\mathbf{g}_q^{\text{H}}\tilde{\mathbf{p}}|^2 \sim \text{Exp}(\frac{1}{\Omega_g})$. Utilizing (6), (8), and (10) with few algebraic manipulations, we can write the CDFs of instantaneous SINRs as

$$\mathbb{F}_{Y_1}(\tau_1) = 1 - \exp\left(-\frac{\tau_1}{\rho_B\Omega_g\eta_1}\right), \tag{47}$$

where $Y_1 \in Y$, $Y \equiv \{\gamma_{q,\mathbb{K}}, \gamma_{q,\mathbb{K}_0}, \gamma_q\}$, and $(\tau_1, \eta_1) \in \mathcal{T}_0$, with $\mathcal{T}_0 \equiv \{(\tau_{\mathbb{K}}, \eta_{\mathbb{K}}), (\tau_{\mathbb{K}_0}, \eta_{\mathbb{K}_0}), (\tau_0, \eta_0)\}$. Similarly, the joint CDFs of instantaneous SINRs at NU can be obtained as

$$\begin{aligned}\mathbb{F}_{Y_1,Y_2}(\tau_1, \tau_2) &= 1 - \exp\left(-\frac{\xi_1}{\rho_B\Omega_g}\right), \\ \mathbb{F}_{Y_1,Y_2,Y_3}(\tau_1, \tau_2, \tau_3) &= 1 - \exp\left(-\frac{\xi_2}{\rho_B\Omega_g}\right),\end{aligned} \tag{48}$$

where $Y_1, Y_2, Y_3 \in Y$, $\xi_1 = \min(\frac{\tau_1}{\eta_1}, \frac{\tau_2}{\eta_2})$ with $(\tau_1, \eta_1), (\tau_2, \eta_2) \in \mathcal{T}_0$ with $(\tau_1, \eta_1) \neq (\tau_2, \eta_2)$, and $\xi_2 = \min(\frac{\tau_1}{\eta_1}, \frac{\tau_2}{\eta_2}, \frac{\tau_3}{\eta_3})$ with $(\tau_i, \eta_i) \in \mathcal{T}_0$, $i = 1, 2, 3$, with $(\tau_i, \eta_i) \neq (\tau_j, \eta_j)$ for all $i \neq j$. Utilizing (47) and (48) in (46), we get the outage probability for the NU.

VI. NUMERICAL RESULTS

In this section, we present the analytical and simulated results for the outage performance of IRS-assisted downlink multi-user multi-group MISO communication system with 2L-HRS. Throughout the numerical results, we have assumed $\theta = 0.43\pi$ and $\epsilon = 1.6$. The continuous phase φ_n is uniformly quantized using a 4-bit quantizer to give $L = 16$

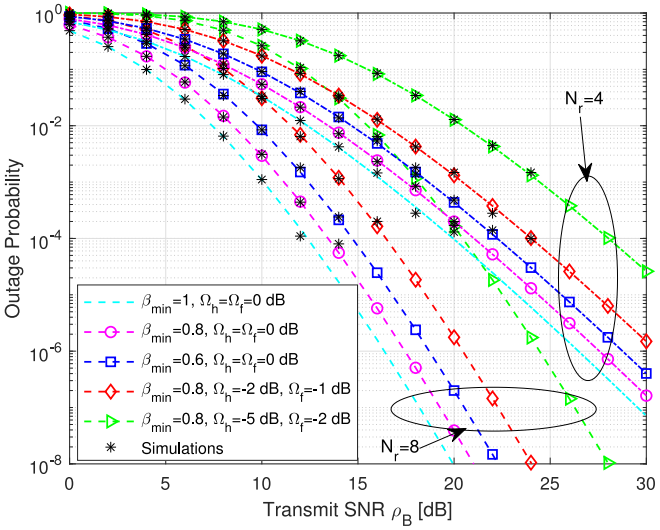

FIGURE 5. Impact of practical reflection amplitude and different channel powers on the performance of considered IRS-assisted four-user downlink MISO environment utilizing 2L-HRS.

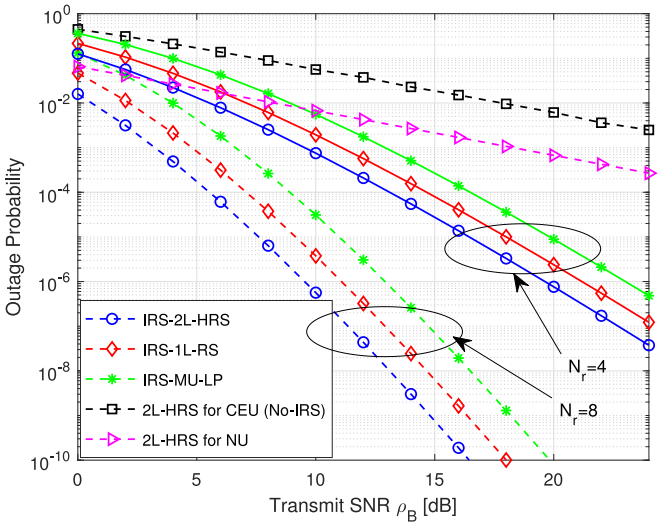

FIGURE 6. Comparison of outage performances for IRS-assisted downlink MISO system with BS utilizing 2L-HRS, 1L-RS, and MU-LP having $K = 4$ users.

discrete levels. The continuous phase φ_n is randomly generated using Uniform distribution between $-\pi$ and π and the n-th reflection amplitude is evaluated by numerically averaging 10^5 iterations of φ_n. Unless mentioned explicitly, we take $N_s = 4$ and $K = 4$ (i.e., four user downlink scenario) with equal number of NUs and CEUs (i.e., $K_0 = 2$). Both the CEUs are considered to be in a single group making $M = 1$ and $K_1 = 2$. It is assumed that 25% of the total transmit power ($\mathcal{P}_B$) is assigned to common data precoder $\mathbf{p}_{\mathbb{K}}$, (i.e., $\alpha_{\mathbb{K}} = 0.25$). However, the common-to-group data precoders $\mathbf{p}_{\mathbb{K}_0}$ and $\mathbf{p}_{\mathbb{K}_1}$ for groups G_0 and G_1, respectively are assigned a power of $0.1\mathcal{P}_B$ and $0.2\mathcal{P}_B$, respectively. The remaining 45% of the power is divided among all private precoding vectors, such that $\sum_{k=1}^{K} \alpha_k = 0.45$. For all the results presented in this section (except Fig. 8), we consider $D_r = 1$ (or, $L_r = N_r$).

Fig. 5 shows the outage performance of a CEU in the IRS-assisted downlink four-user scenario with the BS utilizing 2L-HRS. The impact of practical reflection amplitude and phase shift at IRS element is shown on the outage performance of the CEU by fixing $\Omega_h = \Omega_f = 1$. We also assume equal threshold SINRs for all three SINRs, i.e., $\tau_{\mathbb{K}} = \tau_{\mathbb{K}_1} = \tau_0 = 0.2$. It can be observed from Fig. 5 that outage performance deteriorates with larger deviation of practical reflection amplitude from ideal conditions (i.e., $\beta_{\min} = 1$). Further, it can be noticed that the performance loss (due to practical reflection amplitude) is more for $N_r = 8$ as compared to that for $N_r = 4$.

Furthermore, we have examined the outage performance of the considered IRS-assisted network for varying channel conditions of the BS-IRS and IRS-CEU channels with $N_r = 4, 8$ in Fig. 5. For this, we have set $\beta_{\min} = 0.8$ and have considered $(\Omega_h, \Omega_f) = (0.631, 0.7943)$ and $(0.3162, 0.631)$. Intuitively, the outage performance degrades with the degradation of average channel powers for both the BS-IRS and IRS-CEU channels. Again, the degradation is higher for larger number of reflecting elements at IRS. It is clear from Fig. 5 that the all the analytical curves are matching with the simulated performance. It clearly depicts that the analytical expression of the CEU outage probability obtained through (17) is applicable to arbitrary values of Ω_h, Ω_f and $\beta_{\min}$.

Fig. 6 shows a comparison of outage performances for IRS-assisted 2L-HRS scheme with IRS-assisted 1L-RS and multi-user linear precoding (MU-LP) schemes. In 1L-RS scheme, the data of each user is divided in two parts, i,e, common and private parts. However, in MU-LP scheme, no common message is generated. Thus, we set $\alpha_{\mathbb{K}_0} = \alpha_{\mathbb{K}_1} = 0$ for 1L-RS and $\alpha_{\mathbb{K}} = \alpha_{\mathbb{K}_0} = \alpha_{\mathbb{K}_1} = 0$ for MU-LP in Fig. 6. We have considered $\Omega_h = \Omega_f = 1$ and $\beta_{\min} = 0.8$. It is clear from Fig. 6 that the 2L-HRS with IRS outperforms all the other schemes considered in the figure. Furthermore, we compare the IRS-assisted 2L-HRS scheme with no-IRS situation, where the BS directly communicates to the CEUs by utilizing 2L-HRS. It can be noticed from Fig. 6 that the use of IRS significantly enhances the performance of MISO downlink scenario. In addition, we have shown the outage performance of an NU in a 4-user based MISO system assuming that the average channel power (Ω_g) of BS-NU channel is 15 dB. It can be observed from Fig. 6 that the use of IRS enables a CEU to outperform the NU significantly.

The impact of channel estimation errors (for both BS-IRS and IRS-CEU channels) on the outage performance of the considered network is shown in Fig. 7. We have considered two different settings for average channel gains of BS-IRS$_m$ and IRS$_m$-CEU$_k$ as (i) $\Omega_h = \Omega_f = 0$ dB, and (ii) $\Omega_h = -2$ dB, $\Omega_f = -1$ dB. The error variance of channel estimation error in estimating the channel between the BS and m-th IRS is defined as $\sigma_{h,e}^2 = \mathbb{E}[||\mathbf{H}_m - \hat{\mathbf{H}}_m||^2]$,

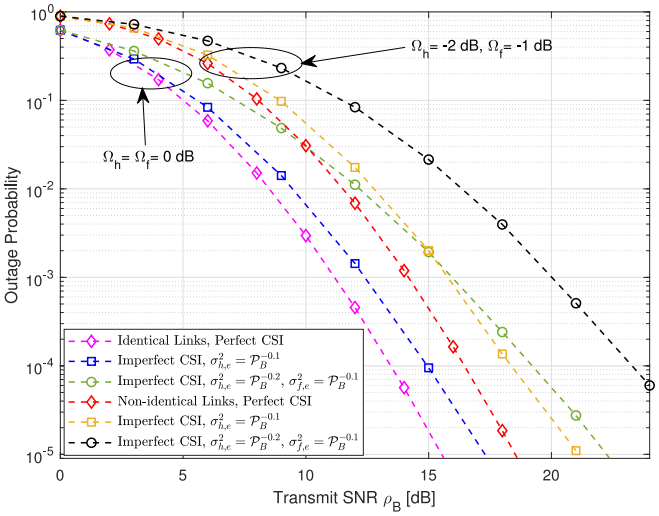

FIGURE 7. Impact of channel estimation errors on the outage performance of the proposed IRS-assisted framework with 2L-HRS for $K = 4$ and $N = 8$.

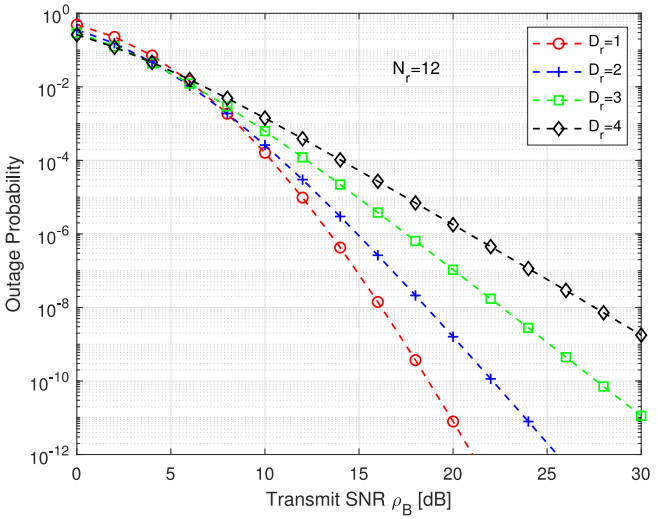

FIGURE 8. Outage probability versus average transmit SNR for different values of D_r with $N_r = 12$ and $\tau_{\mathbb{K}} = \tau_{\mathbb{K}_1} = \tau_0 = 0.2$.

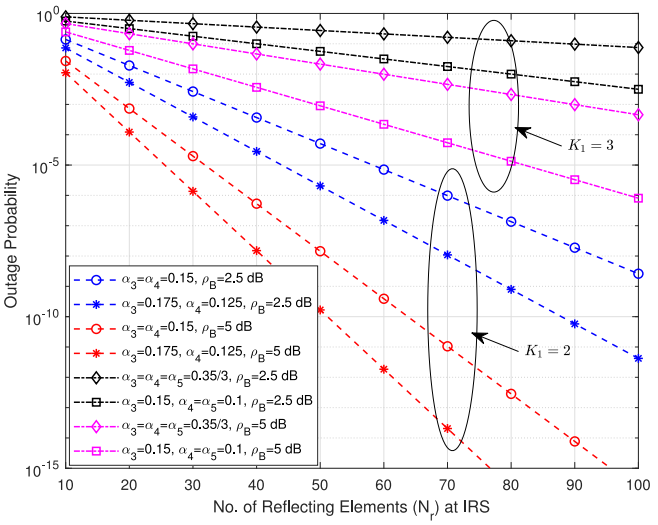

FIGURE 9. Outage probability versus number of reflecting elements (N_r) for $K_1 = 2$ (with $\alpha_{\mathbb{K}_1} = 0.2$) and $K_1 = 3$ (with $\alpha_{\mathbb{K}_1} = 0.15$).

where $\hat{\mathbf{H}}_m$ is the estimated channel matrix corresponding to actual channel matrix $\mathbf{H}_m$. Similarly, we define the estimation error variance for the channel between m-th IRS and k-th CEU as $\sigma^2_{f,e} = \mathbb{E}[||\mathbf{f}_{m,k} - \hat{\mathbf{f}}_{m,k}||^2]$. In Fig. 7, we have taken three different conditions for channel estimation errors (a) $\sigma^2_{h,e} = \sigma^2_{f,e} = 0$, i.e., perfect channel state information (CSI) of both BS-IRS and IRS-CEU channels are available at CEU, (b) $\sigma^2_{h,e} = \mathcal{P}_B^{-0.1}$, $\sigma^2_{f,e} = 0$, i.e., imperfect CSI of BS-IRS channel only, and (c) $\sigma^2_{h,e} = \mathcal{P}_B^{-0.2}$, $\sigma^2_{f,e} = \mathcal{P}_B^{-0.1}$, i.e., imperfect CSI of both BS-IRS and IRS-CEU channels. It can be observed from Fig. 7 that the performance degradation due to condition (b) is small as compared to that due to condition (c) for both the identical and non-identical average channel power scenarios. For example, to attain an outage probability of 0.01 with $\Omega_h = \Omega_f = 0$ dB, an additional transmit SNR (with respect to the perfect CSI condition (a)) of approximately 1 dB and 3.5 dB is required under conditions (b) and (c), respectively. However, if we consider $\Omega_h = -2$ dB, $\Omega_f = -1$ dB, then the same outage probability is achieved at a transmit SNR expense of approximately 1.5 dB and 5 dB under conditions (b) and (c), respectively. Further, it should be noted that the transmit SNR requirement further increases as we set the lower outage probability constraints.

Fig. 8 illustrates the impact of D_r on the outage performance of IRS-assisted 2L-HRS framework with $K = 4$ and $N_r = 12$. It can be observed that for all the transmit SNR (ρ_B) values, the outage probability improves with decreasing D_r and the best outage performance is achieved for $D_r = 1$. In addition, it can be noticed from Fig. 8 that the diversity gain improves significantly as L_r increases.

In Fig. 9, we have shown the outage performance of a CEU with respect to the number of reflecting elements N_r at IRS for four-user ($K = 4$) and five-user ($K = 5$) scenarios with different values of ρ_B. We have assumed two NUs in both the scenarios and only one CEU group (i.e., $M = 1$). It can be observed from Fig. 9 that for all the parameters considered in the figure, the outage performance of a CEU enhances with increasing N_r. This is due to the fact that higher value of N_r provides larger degrees of freedom for reflecting the data received by the BS. Furthermore, it can be noticed from Fig. 9 that the performance of a CEU deteriorates if we put an additional CEU in the same group. The behavior is intuitive as more CEUs in a group will result in large interference power. It can be deduced from Fig. 9 that outage probability versus reflecting element performance of a CEU depends significantly on two parameters, (i) transmit SNR ρ_B and (ii) fraction of the power allocated to the concerned CEU. In Fig. 9, we have assumed that users with indices 1 and 2 are NUs and remaining users are CEUs. We have set $\alpha_{\mathbb{K}} = 0.25, \alpha_{\mathbb{K}_0} = 0.1$, and $\alpha_1 = \alpha_2 = 0.075$ under

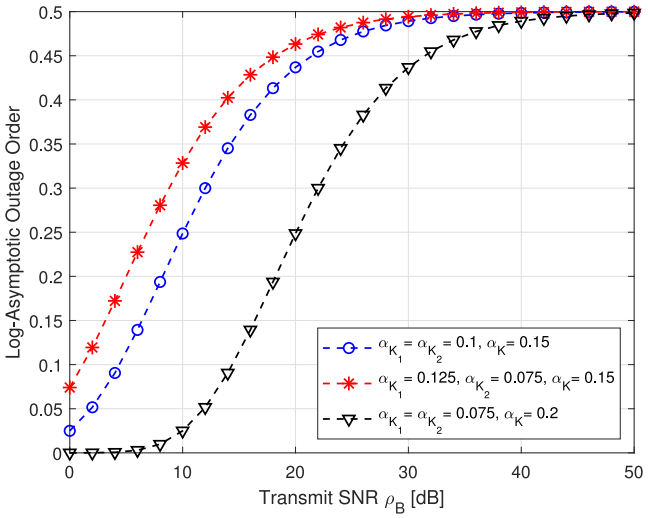

FIGURE 10. Log-Asymptotic Outage Order for sufficiently large number of reflecting elements (i.e., $N_r \to \infty$) for 20 user scenario with 4 NUs ($K_0 = 4$ with $\alpha_{\mathbb{K}_0} = 0.05$) and 16 CEUs ($K_1 = K_2 = 8$).

both four-user and five-user scenarios. In order to evaluate the performance of a CEU (say user 3) we have considered two conditions, (a) uniform power distribution among CEUs and (b) non-uniform power distribution with higher power to user 3, with fixed $\alpha_{\mathbb{K}_1}$. It can be seen from Fig. 9 that the performance of user 3 enhances by allocating more power to the private data of user 3 as well as with high transmit SNR. Moreover, the performance gain is high under two-CEU case as compared to three-CEU scenario.

Fig. 10 shows the variations of Log-Asymptotic Outage Order for large values of N_r with respect to transmit SNR at the BS. For this figure, we consider a dense network with 20 users out of which 16 are close to the cell boundary. These 16 CEUs are equally grouped into 2 groups G_1 and G_2. It is assumed that all the users within a group have equal power allocation coefficients. We also assume $\tau_{\mathbb{K}} = \tau_{\mathbb{K}_1} = 0.1, \tau_0 = 0.01$, and $L_r = N_r$. In Fig. 10, the Log-Asymptotic Outage Order of k-th CEU, $k \in \mathbb{K}_1$ is examined for different values of common-to-group and common-to-all power allocation coefficients. It can be noticed from Fig. 10 that for all the parameter settings considered in the figure, $\mathcal{O}^k_{N_r}$ increases with ρ_B upto certain limit and then saturates at 0.5, which means that $\mathcal{O}^k_{N_r} \leq 0.5$ under all parameter settings. Furthermore, it can be observed from Fig. 10 that increasing the common-to-group power allocation coefficient of G_1 (i.e., the group in which the user under consideration exists) provides improved $\mathcal{O}^k_{N_r}$ values for a fixed common-to-all power. However, if we reduce the common-to-group power by say 25% (for each group G_1 and G_2), and increase the common-to-all power by the same amount (i.e., 50%), then the performance degrades significantly. Thus, it can be deduced from Fig. 10 that the impact of common-to-group power is higher on the overall performance as compared to the impact of common-to-all power, specially under the conditions of large reflecting elements.

VII. CONCLUSION

In this paper, we have considered multiple IRS-assisted downlink MISO HRS communication network and deployed a RS transmission strategy at the BS. Next, an On-Off scheme for controlling the IRSs with practical phase shifts has been proposed. In addition, we have derived the closed-form expressions of outage probability for both cell-edge users and near users by considering both common as well as private data SINR. Through Monte Carlo simulations, we have shown the effectiveness of the proposed scheme and demonstrated that the proposed design framework outperforms the corresponding 1L-RS, MU-LP and 2L-HRS without IRS. Moreover, the impact of channel estimation errors and increasing the number of reflecting elements N_r and number of cell-edge users K_m on the outage probability performance has been unveiled.

REFERENCES

[1] F. Boccardi, R. W. Heath, A. Lozano, T. L. Marzetta, and P. Popovski, "Five disruptive technology directions for 5G," *IEEE Commun. Mag.*, vol. 52, no. 2, pp. 74–80, Feb. 2014.

[2] O. Y. Kolawole, S. Biswas, K. Singh, and T. Ratnarajah, "Transceiver design for energy-efficiency maximization in mmWave MIMO IoT networks," *IEEE Trans. Green Commun. Netw.*, vol. 4, no. 1, pp. 109–123, Mar. 2020.

[3] H. Hashida, Y. Kawamoto, and N. Kato, "Intelligent reflecting surface placement optimization in air-ground communication networks toward 6G," *IEEE Wireless Commun.*, vol. 27, no. 6, pp. 146–151, Dec. 2020.

[4] N. Rajatheva *et al.* "White paper on broadband connectivity in 6G," 2020. [Online]. Available: https://arxiv.org/abs/2004.14247

[5] N. Rajatheva *et al.*, "Scoring the terabit/s goal: Broadband connectivity in 6G," 2020. [Online]. Available: https://arxiv.org/abs/2008.07220

[6] S. Zeng *et al.* "Reconfigurable intelligent surfaces in 6G: Reflective, transmissive, or both?," 2021. [Online]. Available: https://arxiv.org/abs/2102.06910

[7] M. Di Renzo *et al.*, "Smart radio environments empowered by reconfigurable AI meta-surfaces: An idea whose time has come," *J. Wireless Commun. Netw.*, vol. 2019, Mar. 2019, Art. no. 129.

[8] A. S. de Sena *et al.*, "What role do intelligent reflecting surfaces play in multi-antenna non-orthogonal multiple access?," *IEEE Wireless Commun.*, vol. 27, no. 5, pp. 24–31, Oct. 2020.

[9] Q. Wu and R. Zhang, "Towards smart and reconfigurable environment: Intelligent reflecting surface aided wireless network," *IEEE Commun. Mag.*, vol. 58, no. 1, pp. 106–112, Jan. 2020.

[10] E. Basar, M. Di Renzo, J. De Rosny, M. Debbah, M.-S. Alouini, and R. Zhang, "Wireless communications through reconfigurable intelligent surfaces," *IEEE Access*, vol. 7, pp. 116753–116773, Aug. 2019.

[11] S. Gong *et al.*, "Toward smart wireless communications via intelligent reflecting surfaces: A contemporary survey," *IEEE Commun. Surveys Tuts.*, vol. 22, no. 4, pp. 2283–2314, 4th Quart., 2020, doi: 10.1109/COMST.2020.3004197.

[12] E. Basar, "Reconfigurable intelligent surface-based index modulation: A new beyond MIMO paradigm for 6G," *IEEE Trans. Commun.*, vol. 68, no. 5, pp. 3187–3196, May 2020.

[13] C. Huang, A. Zappone, G. C. Alexandropoulos, M. Debbah, and C. Yuen, "Reconfigurable intelligent surfaces for energy efficiency in wireless communication," *IEEE Trans. Wireless Commun.*, vol. 18, no. 8, pp. 4157–4170, Aug. 2019.

[14] M. Di Renzo *et al.*, "Smart radio environments empowered by reconfigurable intelligent surfaces: How it works, state of research, and the road ahead," *IEEE J. Sel. Areas Commun.*, vol. 38, no. 11, pp. 2450–2525, Nov. 2020.

[15] H. Shen, W. Xu, S. Gong, C. Zhao, and D. W. K. Ng, "Beamforming optimization for IRS-aided communications with transceiver hardware impairments," *IEEE Trans. Commun.*, vol. 69, no. 2, pp. 1214–1227, Feb. 2021, doi: 10.1109/TCOMM.2020.3033575.

[16] H. Xie, J. Xu, and Y.-F. Liu, "Max-min fairness in IRS-aided multi-cell MISO systems with joint transmit and reflective beamforming," *IEEE Trans. Wireless Commun.*, vol. 20, no. 2, pp. 1379–1393, Feb. 2021, doi: 10.1109/TWC.2020.3033332.

[17] F. Fang, Y. Xu, Q.-V. Pham, and Z. Ding, "Energy-efficient design of IRS-NOMA networks," *IEEE Trans. Veh. Technol.*, vol. 69, no. 11, pp. 14088–14092, Nov. 2020, doi: 10.1109/TVT.2020.3024005.

[18] D. Xu, X. Yu, Y. Sun, D. W. K. Ng, and R. Schober, "Resource allocation for IRS-assisted full-duplex cognitive radio systems," *IEEE Trans. Commun.*, vol. 68, no. 12, pp. 7376–7394, Dec. 2020, doi: 10.1109/TCOMM.2020.3020838.

[19] M.-M. Zhao, A. Liu, Y. Wan, and R. Zhang, "Two-timescale beamforming optimization for intelligent reflecting surface aided multiuser communication with QoS constraints," [Online]. Available: https://arxiv.org/abs/2011.02237

[20] D. Gunasinghe, D. Kudathanthirige, and G. A. A. Baduge, "Performance analysis of intelligent reflective surface aided wireless communications," [Online]. Available: https://arxiv.org/abs/2010.12544

[21] M. Zeng, X. Li, G. Li, W. Hao, and O. A. Dobre, "Sum rate maximization for IRS-assisted uplink NOMA," *IEEE Commun. Lett.*, vol. 25, no. 1, pp. 234–238, Jan. 2021, doi: 10.1109/LCOMM.2020.3025978.

[22] Z. Ding and H. Vincent Poor, "A simple design of IRS-NOMA transmission," *IEEE Commun. Lett.*, vol. 24, no. 5, pp. 1119–1123, May 2020.

[23] Q. Wu and R. Zhang, "Intelligent reflecting surface enhanced wireless network via joint active and passive beamforming," *IEEE Trans. Wireless Commun.*, vol. 18, no. 11, pp. 5394–5409, Nov. 2019.

[24] Q. Wu and R. Zhang, "Joint active and passive beamforming optimization for intelligent reflecting surface assisted SWIPT under QoS constraints," *IEEE J. Sel. Areas Commun.*, vol. 38, no. 8, pp. 1735–1748, Aug. 2020.

[25] G. Zhou, C. Pan, H. Ren, K. Wang, M. Di Renzo, and A. Nallanathan, "Robust beamforming design for intelligent reflecting surface aided MISO communication systems," *IEEE Wireless Commun. Lett.*, vol. 9, no. 10, pp. 1658–1662, Oct. 2020.

[26] W. Huang, Y. Zeng, and Y. Huang. "Achievable rate region of MISO interference channel aided by intelligent reflecting surface," 2020. [Online]. Available: arXiv:2005.09197

[27] C. Pan *et al.*, "Multicell MIMO communications relying on intelligent reflecting surfaces," *IEEE Trans. Wireless Commun.*, vol. 19, no. 8, pp. 5218–5233, Aug. 2020.

[28] W. Jiang, Y. Zhang, J. Wu, W. Feng, and Y. Jin, "Intelligent reflecting surface assisted secure wireless communications with multiple-transmit and multiple-receive antennas," *IEEE Access*, vol. 8, pp. 86659–86673, May 2020.

[29] W. Yan, X. Yuan, Z. He, and X. Kuai, "Passive beamforming and information transfer design for reconfigurable intelligent surfaces aided multiuser MIMO systems," *IEEE J. Sel. Areas Commun.*, vol. 38, no. 8, pp. 1793–1808, Aug. 2020, doi: 10.1109/JSAC.2020.3000811.

[30] B. Clerckx, H. Joudeh, C. Hao, M. Dai, and B. Rassouli, "Rate splitting for MIMO wireless networks: A promising PHY-layer strategy for LTE evolution," *IEEE Commun. Mag.*, vol. 54, no. 5, pp. 98–105, May 2016.

[31] H. Joudeh and B. Clerckx, "Robust transmission in downlink multiuser MISO systems: A rate-splitting approach," *IEEE Trans. Signal Process.*, vol. 64, no. 23, pp. 6227–6242, Dec. 2016.

[32] Y. Mao, B. Clerckx, and V. O. K. Li, "Rate-splitting multiple access for downlink communication systems: Bridging, generalizing, and outperforming SDMA and NOMA," *J. Wireless Com. Network*, vol. 2018, May 2018, Art. no. 133.

[33] M. Dai, B. Clerckx, D. Gesbert, and G. Caire, "A rate splitting strategy for massive MIMO with imperfect CSIT," *IEEE Trans. Wireless Commun.*, vol. 15, no. 7, pp. 4611–4624, Jul. 2016.

[34] A. R. Flores, R. C. de Lamare, and B. Clerckx, "Linear precoding and stream combining for rate splitting in multiuser MIMO systems," *IEEE Commun. Lett.*, vol. 24, no. 4, pp. 890–894, Apr. 2020.

[35] Y. Mao and B. Clerckx, "Beyond dirty paper coding for multi-antenna broadcast channel with partial CSIT: A rate-splitting approach," *IEEE Trans. Commun.*, vol. 68, no. 11, pp. 6775–6791, Nov. 2020, doi: 10.1109/TCOMM.2020.3014153.

[36] Y. Mao, B. Clerckx, J. Zhang, V. O. K. Li, and M. A. Arafah, "Max-min fairness of K-user cooperative rate-splitting in MISO broadcast channel with user relaying," *IEEE Trans. Wireless Commun.*, vol. 19, no. 10, pp. 6362–6376, Oct. 2020.

[37] A. Z. Yalcin, M. Yuksel, and B. Clerckx, "Rate splitting for multi-group multicasting with a common message," *IEEE Trans. Veh. Technol.*, vol. 69, no. 10, pp. 12281–12285, Oct. 2020, doi: 10.1109/TVT.2020.3006347.

[38] L. You, L. Lei, D. Yuan, S. Sun, S. Chatzinotas, and B. Ottersten, "A framework for optimizing multi-cell NOMA: Delivering demand with less resource," in *Proc. IEEE GLOBECOM*, Dec. 2017, pp. 1–7.

[39] L. You, D. Yuan, L. Lei, S. Sun, S. Chatzinotas, and B. Ottersten, "Resource optimization with load coupling in multi-cell NOMA," *IEEE Trans. Wireless Commun.*, vol. 17, no. 7, pp. 4735–4749, Jul. 2018.

[40] S. Abeywickrama, R. Zhang, Q. Wu, and C. Yuen, "Intelligent reflecting surface: Practical phase shift model and beamforming optimization," *IEEE Trans. Commun.*, vol. 68, no. 9, pp. 5849–5863, Sep. 2020.

[41] A. Papoulis and S. U. Pillai, *Probability, Random Variables, and Stochastic Processes*, 4th ed. New York, NY, USA: McGraw-Hill, 2002.

[42] C. Chesneau, "A New Family of Distributions Based on the Hypoexponential Distribution with Fitting Reliability Data," *Statistica*, vol. 78, no. 2, pp. 127–147, Oct. 2018.

[43] I. S. Gradshteyn and I. M. Ryzhik, *Table of Integrals, Series and Products*, 6th ed. New York, NY, USA: Academic Press, 2000.

ANKUR BANSAL (Member, IEEE) received the master's degree in signal processing from the Division of ECE, NSIT, Delhi, in 2009, and the Ph.D. degree from the Department of Electrical Engineering, Indian Institute of Technology Delhi, India, in 2013. He served as an Assistant Professor with the Division of ECE, NSIT, from September 2013 to December 2019. He has been working as an Assistant Professor with the Department of Electrical Engineering, IIT Jammu, since December 2019. Moreover, he has published several research papers in reputed international journals, such as IEEE TRANSACTIONS ON VEHICULAR TECHNOLOGY, IEEE TRANSACTIONS ON WIRELESS COMMUNICATIONS, *IET Communications*, and IEEE/OSA JOURNAL OF OPTICAL COMMUNICATIONS AND NETWORKING. He has also presented papers in various conferences, such as IEEE VTC, IEEE ICC, IEEE SPCOM, and NCC. His main research interests include multiple-input multiple-output (MIMO) communications, multi-user communications with energy harvesting in UAV-assisted networks, free space optical communications, and intelligent reflecting surface (IRS) assisted communication systems. He has also served as a reviewer of various IEEE journals and conferences.

KESHAV SINGH (Member, IEEE) received the M.Sc. degree in information and telecommunications technologies from Athens Information Technology, Greece, in 2009, and the Ph.D. degree in communication engineering from National Central University, Taiwan, in 2015. He currently works with the Institute of Communications Engineering, National Sun Yat-sen University, Taiwan, as an Assistant Professor. Prior to this, he held the position of Research Associate with the Institute of Digital Communications, University of Edinburgh, U.K., from 2016 to 2019. From 2019 to 2020, he was associated with the University College Dublin, Ireland, as a Research Fellow. He leads research in the areas of green communications, resource allocation, full-duplex radio, ultra-reliable low-latency communication, non-orthogonal multiple access, wireless edge caching, machine learning for communications, and large intelligent surface-assisted communications.

CHIH-PENG LI (Fellow, IEEE) received the B.S. degree in physics from National Tsing Hua University, Hsin Chu, Taiwan, in June 1989, and the Ph.D. degree in electrical engineering from Cornell University, Ithaca, NY, USA, in December 1997.

From 1998 to 2000, he was a Member of Technical Staff with Lucent Technologies. From 2001 to 2002, he was the Manager of Acer Mobile Networks. Since 2002, he has been with National Sun Yat-sen University (NSYSU), Kaohsiung, Taiwan, where he is currently a Distinguished Professor of the Institute of Communications Engineering. He has served various positions with NSYSU, including the Chairman of Electrical Engineering Department, the VP of General Affairs, the Dean of Engineering College, and the VP of Academic Affairs. His research interests include wireless communications, baseband signal processing, and data networks. He is currently the Director General with the Engineering and Technologies Department, Ministry of Science and Technology, Taiwan. He is currently the Chapter Chair of IEEE Broadcasting Technology Society Tainan Section. He has also served as the Chapter Chair of IEEE Communication Society Tainan Section, the President of Taiwan Institute of Electrical and Electronics Engineering, an Editor of IEEE TRANSACTIONS ON WIRELESS COMMUNICATIONS, an Associate Editor of IEEE TRANSACTIONS ON BROADCASTING, the General Chair of 2020 Taiwan Telecommunications Annual Symposium, the General Co-Chair of 2017 IEEE Information Theory Workshop, the General Chair of 2014 IEEE 11th VTS Asia Pacific Wireless Communications Symposium, and the Member of Board of Governors with IEEE Tainan Section.